IN-02

1705

841

Summary of In-Flight Flow Visualization Obtained From the NASA High Alpha Research Vehicle

David F. Fisher, John H. Del Frate, and Fanny A. Zuniga

January 1991

NASA
National Aeronautics and
Space Administration

Summary of In-Flight Flow Visualization Obtained From the NASA High Alpha Research Vehicle

David F. Fisher, John H. Del Frate, and Fanny A. Zuniga
Dryden Flight Research Facility, Edwards, California

1991

SUMMARY OF IN-FLIGHT FLOW VISUALIZATION OBTAINED FROM THE NASA HIGH ALPHA RESEARCH VEHICLE

David F. Fisher, John H. Del Frate, and Fanny A. Zuniga
NASA Ames Research Center
Dryden Flight Research Facility
Edwards, CA

ABSTRACT

A summary of the surface and off-surface flow visualization results obtained in flight on the F-18 high alpha research vehicle (HARV) is presented, highlighting the extensive three-dimensional vortical flow on the aircraft at angles of attack up to 50°. The emitted fluid technique, as well as tufts and flow cones, were used to document the surface flow. A smoke generator system injected smoke into the vortex cores generated by the forebody and leading-edge extensions (LEXs). Documentation was provided by onboard still photographs and video, by air-to-air photography, and by postflight photography.

The surface flow visualization techniques revealed laminar separation bubbles near the forebody apex, lines of separation on the forebody and LEX, and regions of attached and separated flow on the wings and fins. The off-surface flow visualization techniques showed the path of the vortex cores on the forebody and LEX as well as the LEX vortex core breakdown location. An interaction between the forebody and LEX vortices was noted. The flow over the surfaces of the vertical tail was categorized into regions of attached, unsteady, or separated flow using flow tufts.

INTRODUCTION

Recently, expanding the envelope of fighter aircraft to include controlled flight at high angles of attack has been emphasized. Fighter aircraft such as the F-18 and F-16 use leading-edge extensions (LEXs) or wing body strakes which provide vortex lift at moderate to high angles of attack (ref. 1). However, the prediction and control of the vortical lift from these devices and the mutual interactions of the vortices are not well understood. The combined effect of the LEX or wing body strake vortices and the forebody vortices on the vehicle aerodynamics must be integrated productively to avoid stability and control problems.

Understanding the vortical flow interactions by studying scale models in wind tunnels can be difficult. Experimental wind-tunnel results with different scale models can give conflicting results, even when tested at the same Reynolds number (ref. 2). In early subscale model tests, the interaction of the forebody and LEX vortices on 6-percent and 7-percent scale F-18 models resulted in apparent lateral stability for all angles of attack, including stall and post-stall regions. However, flight data and wind-tunnel results for the large-scale (16 percent) model at low Reynolds numbers indicated a region of instability near maximum lift. Data from later, more comprehensive wind-tunnel tests of these same models in the present F-18 configuration (LEX slots filled and maximum leading-edge flap deflection at −34°) still show some differences, but the increments are greatly reduced. Understanding such scale, model, wind-tunnel-to-wind-tunnel, and wind-tunnel-to-flight effects are essential for successful design of future fighter aircraft intended to operate at high angles of attack.

The National Aeronautics and Space Administration (NASA) is currently conducting a High Alpha Technology Program (HATP) to provide design guidelines and new concepts for vortex control on advanced, highly maneuverable aircraft at high angles of attack. This program, which uses the F-18 aircraft for validation and demonstration, consists of wind-tunnel tests of subscale (refs. 3 and 4) and full-scale models and components, calibration for computational fluid dynamics (CFD) techniques codes (refs. 5–9), piloted simulations, and full-scale flight testing (refs. 10–20).

As part of this investigation, the Ames Research Center's Dryden Flight Research Facility has been conducting extensive flow visualization studies on the F-18 high alpha research vehicle (HARV). Surface and off-surface flow visualization results have been obtained in flight at low speeds on the F-18 HARV. These results highlight the extensive vortical three-dimensional, separated flow on the aircraft at angles of attack up to 50°. The surface flow on the forebody and LEX have been visualized using the emitted fluid technique described in references 10–13. Tufts and flow cones have also been used to observe the surface flow on the wing, LEX, and vertical tails. The off-surface vortical flows from the forebody and LEX have been visualized by injecting smoke from a smoke generation system into the vortex cores (refs. 16–17). This paper summarizes the results of this flow visualization to date.

NOMENCLATURE

b	aircraft span, ft
BART	Basic Aerodynamic Research Tunnel, Langley Research Center
$C_{n\beta}$ dynamic	departure resistance parameter, per deg
C_L	lift coefficient
DTRC	David Taylor Research Center (7- by 10-ft wind tunnel)
F.S.	fuselage station, in. (nose apex at 59.82 in.)
FVF	Flow Visualization Facility, Dryden Flight Research Facility
HARV	high alpha research vehicle
ℓ	aircraft length from the nose apex to nozzle exhaust plane, 54.4 ft
l.e.	leading edge
LEX	leading-edge extension
LSB	laminar separation bubble
LSWT	Low Speed Wind Tunnel, McDonnell Aircraft Company
M_∞	free-stream Mach number
NATOPS	Naval Air Training and Operating Procedures Standardization
PGME	propylene glycol monomethyl ether
R	reattachment line location
$R_{\theta_{a.l.}}$	Reynolds number based on the momentum thickness at the attachment line for a cylinder $R_{\theta_{a.l.}} \approx \dfrac{(0.403)\sin\lambda \left(\frac{Re_d}{7}\right)^{\frac{1}{2}}}{(2\cos\lambda)^{\frac{1}{2}}}$
$Re_{\bar{c}}$	Reynolds number based on mean aerodynamic chord

2

Re_d	Reynolds number based on local diameter
S_1	primary vortex separation line location
S_2	secondary vortex separation line location
S_3	tertiary vortex separation line location
x	length along aircraft longitudinal axis from nose apex, ft
y	location along aircraft lateral axis
α	angle of attack, right wingtip angle-of-attack vane corrected for upwash and angular rates, deg
β	angle of sideslip, average of left and right wingtip sideslip vanes corrected for angle of attack, deg
λ	equivalent forebody sweep angle; $90 - (\alpha - 5.6)$, deg
θ	forebody cross-section angular location ($0°$ is bottom centerline, positive is clockwise as seen from a front view, $0°$ to $360°$), deg

VEHICLE DESCRIPTION

The HARV (fig. 1) is a single-place F-18 aircraft built by McDonnell Douglas and Northrop and is powered by two General Electric (Lynn, Massachusetts) F404-GE-400 afterburning turbofan engines. The aircraft features a midwing with leading-edge (l.e.) and trailing-edge flaps operating on a schedule that is a function of angle of attack. For free-stream Mach number (M_∞) ≤ 0.76 and angle of attack (α) $\geq 26°$, the l.e. flap is down $-33°$ (maximum), and the trailing-edge flap is at $0°$. Leading-edge extensions are mounted on each side of the fuselage from the wing roots to just forward of the windscreen. The aircraft has twin vertical tails canted out from vertical $20°$ and differential all-moving horizontal stabilizers. The F-18 HARV, with the current flight control computers and 8.3.3 programmed read only memory (PROM) set, was flown by NASA in the fighter escort configuration (without stores) for the flights reported herein. The aircraft carried no missiles and the wingtip missile launch racks were replaced with special camera pods and wingtip airdata booms. The flight test noseboom was removed from the aircraft and a flush airdata system installed (ref. 20). The aircraft has an unrestricted angle-of-attack flight envelope in this configuration with the center of gravity between 17- and 25-percent mean aerodynamic chord, as defined by the Naval Air Training and Operating Procedures Standard-ization (NATOPS) manual. For the data reported herein, the LEX fences were not installed.

EXPERIMENT DESCRIPTION AND TEST CONDITIONS

Both off-surface and on-surface flow visualization techniques were used on the F-18 HARV in flight. The off-surface flow visualization technique used a smoke generation system (refs. 16 and 17). This system ducted smoke to the forebody and LEX apexes to mark the forebody and LEX vortex cores, respectively, at high angles of attack. This system is similar to that used by Fennell (ref. 21) on the HP-115 in which a modified marine distress signal cartridge was mounted externally below the wing leading edge. The F-18 system, however, contained up to 12 specially formulated pyrotechnic cartridges (ref. 17) and was mounted internally with the smoke ducted to the LEX or forebody exhaust ports.

Flow visualization data on the HARV were obtained at both steady-state and dynamic flight conditions. Time-correlated onboard video and still cameras were used to document the off-surface flow visualization data. The camera and smoke generator system locations are shown in figure 2. The LEX and forebody smoke ports were located symmetrically on both sides of the airplane. Only the locations on the right side are shown.

The on-surface flow visualization used both the emitted fluid technique (refs. 10 and 22) and flow cones and tufts (refs. 11 and 23). With the emitted fluid technique, a small quantity ($\sim$ 1 qt) of a fluid mixture is slowly emitted out of flush surface orifices while the aircraft is stabilized at the desired conditions. A similar technique was used in flight on the HP-115 (ref. 24) using a different fluid. The fluid used on the HARV, and first used by Belevtsov et al. (ref. 22), was a mixture of propylene glycol monomethyl ether (PGME) and a toluene-based red dye. On the HARV, the technique was used on the aircraft forebody and LEX. On the forebody, the fluid was emitted out of five circumferential rings of orifices (fig. 3(a)); on the left LEX, it was emitted at three rows of orifices (fig. 3(b)). As the fluid flows back along the surface the PGME evaporates, leaving the dye to mark the surface streamlines. This technique required the pilot to stabilize at the test conditions for 75 to 90 sec while the PGME evaporated and the dye set. An uplink guidance system, similar to that described in reference 25, helped the pilot maintain conditions.

Tufts were also used for surface flow visualization. Nylon cord tufts approximately 8 in. long were taped to the surface of the wing, vertical tails, and fuselage, with 5 to 6 in. of tuft protruding from the tape (ref. 11). Flow cones were used in place of the nylon cord tufts for some flights. The flow cones used (refs. 11 and 23) are 3 in. long and are made of plastic covered with reflective tape. The nylon tufts and flow cones were limited to locations aft of the engine inlets. Wool yarn tufts were used on the upper surface of the LEX and fuselage forward of the engine inlets to prevent damage in case any tufts were ingested by the engines.

The data reported were obtained at 1-g steady-state flight conditions, during both zero and wings-level sideslip maneuvers. The nominal altitudes were between 20,000 and 30,000 ft and the Mach numbers varied from approximately 0.2 to 0.4. Data presented were obtained over an angle-of-attack range of 10° to 50° and at sideslip angles up to ±6°.

RESULTS AND DISCUSSION

This section has been divided into four sections: LEX vortex flow visualization, wing surface flow visualization, vertical tails flow visualization, and forebody vortex flow visualization. The LEX vortex flow visualization is discussed first because of the dominant role it plays in the high-angle-of-attack aerodynamics of the F-18 aircraft. The wing surface and the vertical tails flow visualization are discussed next because the LEX vortices have a strong affect on them. Finally, the forebody flow visualization describes the forebody vortical flow and its interaction downstream with the LEX vortical flow field.

The vortical flow on the F-18 configuration is best illustrated using an example from the water tunnel, shown in figure 4. The flow field about the F-18 aircraft at high angles of attack is dominated by much three-dimensional separated flow. Strong, tightly wound vortices are generated by the sharp-edged LEXs, and these vortices cause outward spanwise flow on the inner wing. At 35° angle of attack, the vertical tails are encompassed by turbulent flow caused by the LEX vortex core breakdown. Interactions between the forebody and LEX vortices occur where the flow from the forebody is drawn below the LEX vortex and extends out onto the wing.

4

Leading-Edge Extension Vortex Flow Visualization

The LEX has a significant effect on the high-angle-of-attack characteristics of the F-18 aircraft and contributes significant additional lift caused by separation-induced vortex flows. As shown in figure 5 (ref. 26), at $\alpha = 35°$, the LEX accounts for approximately 22 percent of the total lift of the aircraft although it is only 14 percent of the wing area. These vortical flows were examined using both off-surface and surface flow visualization techniques.

Off-Surface Flow Visualization

Effect of angle of attack.   Off-surface flow visualization of the LEX vortices was obtained by discharging smoke from a 1-in. diameter port near the LEX apex. The smoke was then entrained into the LEX vortex cores. Figure 6 shows examples of flow visualization of the LEX vortex cores for $\alpha = 20.0$, 29.8, and 42.5°. The view is from a 35-mm camera in the right wingtip pod, looking in board at the aircraft fuselage. A strong vortex is generated by the sharp edge of each LEX. The smoke marks only the vortex core and not the complete vortex system; the complete vortex system is much larger and extends down to the aircraft surface (refs. 4 and 18). The in-flight LEX vortex core breakdown locations (ref. 18) are presented in figure 7 as a function of angle of attack and fuselage length. The data show that as the angle of attack increases, the vortex core breakdown point moves nearer the LEX apex. For comparison, data from subscale tests in wind and water tunnels (refs. 4 and 18) are presented and fall within the scatter of the flight data, despite the wide range in Reynolds numbers.

Effect of sideslip.   Figure 8 shows photographs, from the right wingtip camera, of the LEX vortex core breakdown at $\alpha \sim 25°$ during a wings level sideslip maneuver. The right LEX vortex core breakdown position can be seen moving aft as sideslip is decreased from 4.5° (vortex on windward side) to $-3.4°$ (vortex on leeward side), where positive angle of sideslip is flow from the right, or aircraft nose left as viewed by the pilot. Other onboard cameras showed that, at the same time, the leeward vortex core had moved outboard and away from the LEX surface, while the windward vortex core had moved inboard and closer to the LEX surface.

The effect of sideslip on the vortex core breakdown position is summarized in figure 9 for $\alpha \sim 20°$, 25°, and 30°. In this figure, the lateral location of the vortex core breakdown is plotted against longitudinal location of the vortex core breakdown for positive, negative, and 0° sideslip conditions. This data was obtained from the left wingtip and the left vertical tail video cameras. As the figure shows, sideslip has a significant effect on vortex core breakdown position. This effect is most pronounced at a 20° angle of attack, where 5° of sideslip can change the longitudinal vortex core breakdown position by more than 10 percent of the fuselage length. The leeward vortex core moved outboard with sideslip, while the windward vortex core moved inboard.

Surface Flow Visualization With Emitted Fluid Technique

Surface flow visualization was also obtained on the left LEX using the emitted fluid technique. A schematic of the cross-sectional flow about the LEX is shown in the inset of figure 10(a). Only the primary vortex which separates at the sharp edge of the LEX was seen in figures 4, 6, and 8. Secondary

and tertiary vortices, however, are induced by the primary vortex, as shown by separation lines at S_2 and S_3, respectively. Figure 10 shows surface flow visualization results obtained during stabilized flight at $\alpha \sim 30°$ and 47°. The fluid emitted from the orifices mark the surface streamlines which merge into a wide longitudinal band along the upper surface of the LEX. The inboard edge of this band defines the secondary separation line (S_2), while the outboard edge is the result of the tertiary separation line (S_3). The wide band was a weak reattachment zone (ref. 13).

Figure 7 shows that at $\alpha \sim 30°$, vortex core breakdown occurs in flight at $x/\ell \sim 0.43$. This occurs just forward of the last orifice row at F.S. 357 ($x/\ell = 0.454$), as shown in figure 10(a). Forward of this point, the LEX surface flow should be strongly influenced by a strong, tightly wound vortex core. The effects of this tightly wound vortex core are demonstrated by the clearly marked surface flows and well-defined separation lines in figure 10(a). By contrast, at $\alpha \sim 47°$, extrapolating from fig. 7, vortex breakdown occurs somewhere between the LEX apex and the first orifice row at F.S. 253 ($x/\ell = 0.295$). Despite the fact that all three orifice stations are aft of vortex core breakdown, the secondary and tertiary separation lines are still present (fig. 10(b)). The separation lines are somewhat smeared compared to $\alpha \sim 30°$, probably because of the difficulty in stabilizing the aircraft at this angle of attack. The presence of these separation lines in the surface flow visualization for $\alpha = 47°$ indicates the presence of a vortex-type flow field extending far downstream of the vortex core breakdown location. The primary vortex is, however, without a defined core, weak in strength, and dissipating.

Another difference between the surface flow results at $\alpha \sim 30°$ and 47° is that the secondary and tertiary separation lines have moved significantly outboard at F.S. 357 at $\alpha = 47°$. This is probably because of the increased size of the vortex as a result of the vortex core breakdown.

Wing Surface Flow Visualization

As figure 5 shows, the LEX provided a favorable effect on the lift characteristics of the F-18 aircraft above $\alpha \sim 20°$. An effort was made to determine if the effect was caused by the additional lift of the LEX alone or by some synergistic effect derived from the influence of the LEX vortex on the wing flow. To accomplish this, tufts and flow cones were applied to the LEX, wing upper surfaces, and fuselage to visualize the flow patterns and flow interactions on those lifting surfaces. For some flights, the LEX smoke system was used with tufts or flow cones to provide simultaneous visualization of the LEX vortex core path and breakdown location, the wing flow quality, and the interaction between the LEX vortex and the wing flow. The LEX, wing, and l.e. flap flow patterns as well as the LEX–wing interaction will be discussed in the following section.

Figures 11–13 show the results of the wing surface flow visualization from flight at $\alpha \sim 20°$, 25°, and 30°. The interpretation of the surface flow on the wing is shown in the inset. The end of the tuft attached to the surface is shown as a round dot; the dashed lines are the authors' interpretation of the surface flows.

At $\alpha \sim 20°$ (fig. 11 (a)), the vortex core breakdown was just forward and slightly outboard of the vertical tails. The separation line band, similar to that shown by the emitted fluid technique, can be identified on the LEX where the tufts merge. The tuft spacing, however, was not fine enough to identify the secondary separation line from the tertiary separation line, as shown in figure 10. The influence of the LEX vortex system was evident on the inboard portion of the wing, causing the flow to stay attached and the streamlines, in general, to be directed outward and aft. In the figure, the smoke shows only the vortex core and not the total vortex system. An extensive amount of reversed flow and surface vortical flow was present on the main wing just aft of the l.e. flap–wing junction. Evidence indicating the presence of three

6

counterclockwise upper surface vortices can be seen with the tufts near midspan as shown in the inset. Similar upper surface vortices have been observed in a water tunnel on thick wings (ref. 27). Near the wingtip the tufts indicated that a clockwise surface vortex was present. This interpretation of the wing flow was aided by high-speed motion-picture photography filmed at 78 frames/sec. The view of flow cones on the l.e. flap (fig. 11(b)) were obtained from a different flight at nearly identical conditions. At $\alpha \sim 20°$, nearly all of the inboard l.e. flap had attached flow, while the outboard l.e. flap had reversed flow.

Results on the wing at $\alpha \sim 25°$ are shown in figure 12. Again, the separation line band on the LEX can be seen as well as the attached, outward flow on the inboard portion of the wing (fig. 12(a)) caused by the LEX vortex. Much of the flow on the wing directly aft of the wing–l.e. flap junction was reversed, with only one counterclockwise surface vortex on the wing near midspan. The clockwise vortex at the wingtip has moved slightly further aft (fig. 12(a)). At this angle of attack, increasingly more of the inboard l.e. flap (fig. 12(b)) is reversed than at $\alpha \sim 20°$.

At $\alpha \sim 30°$ (fig. 13), the flow on the wing is similar to that at $\alpha \sim 20°$ and 25°. Slightly less of the inboard wing appears to be affected by the LEX vortex (fig. 13(a)), with less attached flow on the inboard wing than at $\alpha \sim 20°$ or 25°. More of the wing has reversed or separated flow. At the higher angle of attack, more of the l.e. flap has separated, or reversed flow, as shown in figures 13(a) and (b).

Vertical Tails Flow Visualization

The F-18 fleet has experienced vertical tail buffet problems at high angles of attack because of the proximity of the vertical tails to the LEX vortex system (refs. 26 and 28). An aerodynamic fix, the LEX fence (refs. 4, 26, and 28), has been retrofitted to the F-18 fleet and has partially alleviated the problem. The data in this paper, however, is without the LEX fence installed.

In addition to the tail buffet problem, the close proximity of the LEX vortices to the fins and rudders also affect the lateral stability and control of the aircraft. In particular, between 35° and 45° angle of attack, the aircraft experiences a region of wing rock (refs. 13 and 14) which the pilots are unable to correct because of limited lateral-directional control power and control phasing difficulties. Above 45° angle of attack, pilot comments indicate that roll damping is increased along with some rudder control power. Figure 14 (from ref. 29) is a plot of the directional divergence parameter as a function of angle of attack. This plot, which was derived from wind-tunnel and flight data, supports the pilots comments. Figure 14 shows that for $\beta \sim 0°$ and between 35° and 43° angle of attack, the aircraft has very poor directional stability but has significant departure resistance at $\alpha > 45°$. Although the F-18 has poor directional stability between 35° and 43° angle of attack, a McDonnell Aircraft Company report by C.R. Hobbs and R.S. Pelikan indicates that with sufficient sideslip ($\beta \geq \pm 8°$), the aircraft generates a restoring moment at $\alpha = 40°$.

To study the effects of the LEX vortex on the fins, the surface flow on both the inboard and outboard surfaces of the fins was studied from 10° to 50° angle of attack at approximately 0° sideslip. The surface flow was studied using both flow cones and tufts on the inboard and outboard surfaces. These were photographed from the right wingtip 35-mm camera and videotaped from the left wingtip camera and an aft-looking turtleback camera. In some cases, data from onboard cameras were supplemented with data from cameras in chase aircraft.

Examples of fin tuft photographs from the right wingtip 35-mm camera are shown in figure 15 for $\alpha \sim 10, 30,$ and 50°. The interpretation of the tuft photos and video are shown in figure 16. Areas

7

without crosshatching indicate attached flow where the tufts were generally stationary in the direction shown. Areas with single crosshatching indicate unsteady flow where the tufts were fluctuating but generally in the direction shown. Areas with double crosshatching indicate separated flow where the direction of the tufts were generally random. Sketches for $\alpha \sim 10°$ to $30°$ (fig. 16(a–d)) include both inboard and outboard surfaces. Sketches for $\alpha > 30°$ are limited to the outboard view because of limited data on the inboard surfaces at these conditions.

At $\alpha \sim 10°$ (fig. 16 (a)), the flow on the fins is attached, except for a small region of unsteady and separated flow at the outboard root near the path of the LEX vortex. As angle of attack is increased to 20° (fig. 16(b)), the area of unsteady and separated flow near the root expands to encompass approximately the lower 50 percent of the outboard surface. The location of the separated flow correlates well with data in figures 6(a) and 7, which indicate that the LEX vortex breakdown is occurring just in front of the fins. The inboard surface was separated at the top, unsteady in the midsection, and attached at the lower section. The separated region was approximately 25 percent, the unsteady region approximately 35 percent, and the attached region approximately 40 percent of total surface area, excluding the rudder.

At $\alpha \sim 25°$ (fig. 16(c)), the flow on the outboard surface of the fin has become completely separated. The area of separated flow on the inboard surface has remained approximately the same. The area of unsteady flow, however, has increased to approximately 45 percent, and the area of attached flow has decreased to approximately 30 percent. At $\alpha \sim 30°$, the flow on the outboard side of the fins is fully separated except for small regions near the root (fig. 16(d)). The flow on the inboard surface is primarily unsteady (55 percent of area), with some separated flow (35 percent of area) near the leading edge and top, and a small attached flow region (10 percent of area) near the root. Reference 28 discussed surface flow visualization results from the vertical stabilizers of a 6-percent scale CF-18 model with a LEX fence using the oil streak technique at $\alpha = 30°$ and $M = 0.6$. The wind-tunnel and flight results show similar areas of chordwise flow on the inboard side of the fin roots and spanwise flow at the trailing edge of the outboard fin roots. Large regions of separated flow on the outboard surface of the fins were also observed for both model and aircraft. For the flight case, the flow direction of the unsteady region on the inboard surface was difficult to ascertain but appeared to be aligned chordwise. The wind-tunnel results were more spanwise, similar to that observed in flight at $\alpha \sim 25°$.

On the outboard surface, as the angle of attack increased from approximately 30° to 50° (fig. 16(d–h)), a small region of spanwise, unsteady, "quasi-attached" flow near the trailing edge of the root expanded to include approximately the last 75 percent of the chord at $\alpha \sim 50°$. As shown in figure 2, the fins were placed on the upper outboard corners of the fuselage between the wing and the horizontal stabilizer. At extreme angles of attack ($\alpha > 44°$), significant flow passes between the trailing edge of the wing and the leading edge of the horizontal stabilizer and attaches to the outboard surface of the fins.

As mentioned previously, the deterioration of the lateral-directional control authority and stability occurs between 35° to 45° angle of attack. The return of some stability and control at angles of attack above 45° correlates with a return of unsteady attached flow on the outboard surface of the fins. Although probably not the forcing mechanism of wing rock encountered on the F-18 HARV, the adverse flow environment of the fins contributes to the aircraft's limited lateral stability and control between 35° and 45° angle of attack and probably aggravates the wing rock.

Forebody Vortex Flow Visualization

At high angles of attack, vortical flow has been observed on the forebody of the F-18 configuration, both in the water tunnel (fig. 4) and in flight (refs. 10–18). In flight, both surface and off-surface flow visualization were used to identify this vortical flow. Smoke was injected into the airstream from ports near the nose apex to visualize the off-surface forebody vortex core paths. Fluid was emitted out of five circumferential orifice rings to trace the surface streamlines on the forebody, in a similar manner to that for the LEX. The results from this flow visualization are discussed in the following paragraphs.

Off-Surface Flow Visualization

Off-surface flow visualization of the right forebody vortex core using smoke injection is shown in figure 17 for angles of attack from 25.3° to 42.5° at near 0° sideslip. At $\alpha = 25.3°$ (fig. 17(a)), the forebody vortices have just begun to form. The vortex core is easily disrupted by the flow about the canopy and becomes unstable. As the angle of attack is increased to $\alpha = 29.5°$ (fig. 17(b)), the vortex core becomes much better defined and coherent, even far past the canopy. With increasing angle of attack (fig. 17 (c–f)), the forebody vortex cores are also lifted further from the surface. This lifting can be seen most clearly by comparing $\alpha = 29.5°$ (fig. 15(b)) with $\alpha = 40.6°$ (fig. 17(e)) and noting the vortex core positions above the forebody forward of the canopy.

Also shown in figure 17 is an interaction between the forebody and LEX vortex cores in which the forebody vortex core is drawn down under the LEX vortex core and is quickly dissipated. Inset sketches of the vortical flow show the location of this interaction. The LEX vortex core sizes and positions were sketched from photos and video of LEX vortex flow visualization that are not presented.

At $\alpha = 29.5°$ (fig. 17(b)), the forebody vortex core is drawn down beneath the LEX vortex just aft of the junction between the LEX and the wing leading-edge flap. As the angle of attack increases, the location of this interaction moves forward (figs. 17(b–f)). The longitudinal location of this interaction is shown in figure 18 as a function of angle of attack.

Also plotted in figure 18, as a crosshatched area, is the approximate LEX vortex core breakdown positions from figure 7. The forebody–LEX vortex core interactions shown for 0° sideslip occur slightly aft of the LEX vortex core breakdown position. The large increase in the size of LEX vortex structure produced by vortex core breakdown causes the LEX and forebody vortices to come much closer. This results in the forebody–LEX vortex core interaction occurring just aft of the vortex core breakdown.

Surface Flow Visualization

Forebody surface flow visualization on the F-18 HARV using the emitted fluid technique is shown in figure 19 for $\alpha \sim 30°$ and 47°. As shown previously for the LEX, the technique marks the surface flow streamlines with a red dye. Where the flow streamlines merge, lines of separation are defined and, conversely, where the streamlines diverge, lines of reattachment are defined. A schematic of the flow about the forebody is shown in the inset of figure 19(a) and identifies pairs of primary and secondary vortices. Only the primary vortex was shown with the smoke flow (fig. 17). Both primary and secondary forebody separation lines are clearly visible in figure 19. At $\alpha \sim 30°$ (fig. 19(a)), the secondary vortex separation line is not apparent on the forebody until about F.S. 142. At $\alpha = 47°$ (fig. 19(b)), however, the

secondary vortex separation line can be seen near F.S. 85. This indicates a stronger, more fully developed vortex system that originates nearer the apex than at $\alpha = 30°$.

In the surface flow visualization on the forebody, a kink in the streamlines was observed near the apex at $\alpha = 30°$ (fig. 19(a)), and was much more extensive at $\alpha = 47°$ (figs. 19(b) and (c)). This kink was caused by a laminar separation bubble where the boundary layer transitions from laminar to turbulent flow. Note that where the boundary layer was prematurely tripped by the screwhead protuberances (fig. 19(c)), there was no kink in the surface streamlines. This laminar separation bubble was somewhat unexpected. Laminar separation bubbles are usually associated with flow in the critical Reynolds number range ($Re_d = 2 \times 10^5$ to 4×10^5) for ogives and circular cylinders (ref. 30). The flight data (ref. 19) was far into the supercritical range, and mostly turbulent flow would be expected.

The amount of laminar flow on the nose at $\alpha = 47°$ was surprising at first glance. However, when the attachment line boundary layer is analyzed in a manner similar to a swept cylinder (ref. 31), or the leading edge of a swept laminar flow wing (ref. 32), an explanation could be made. For a smooth forward-swept cylinder or wing leading edge with a laminar boundary layer at the apex, the attachment line boundary layer would be expected to remain laminar until the momentum thickness Reynolds number at the attachment line, $R_{\theta_{a,l}}$, reached approximately 230 to 240 (ref. 32). At this point, the attachment line boundary layer begins to transition to turbulent flow causing the boundary layer downstream of this location to be turbulent. Consequently, $R_{\theta_{a,l}}$ was calculated for the F-18 radome at the end of the last evidence of the laminar separation bubble at F.S. 103 using the equation in the nomenclature. Because the radome of the F-18 airplane is inclined down 5.6° from the horizontal reference plane, the equivalent sweep angle for the F-18 HARV forebody, λ, was determined to be $90° - (\alpha - 5.6°)$. For the test point at $\alpha = 47°$ and $Re_d = 1.44 \times 10^6$, $R_{\theta_{a,l}}$ was calculated to be approximately 223. This quantity is very nearly equal to the critical $R_{\theta_{a,l}}$ value of 230 to 240 for the smooth-swept cylinders or laminar flow wing leading edges. $R_{\theta_{a,l}}$ for the test point at $\alpha = 30°$ did not show as good a correlation. For this point, $R_{\theta_{a,l}}$ was calculated to be 275 for the end of the laminar separation bubble at F.S. 74. This is significantly higher than the critical value. However, the equation assumes a constant diameter leading edge, and there may be effects because of the changing forebody diameter as well as other tip effects.

CONCLUDING REMARKS

In-flight flow visualization results of the vortical flow on the forebody, leading-edge extensions (LEXs), wings, and vertical stabilizers have been summarized for the F-18 high alpha research vehicle (HARV) for angles of attack up to 50°. Smoke injection was used to visualize the off-surface forebody and LEX vortical flow characteristics. An emitted fluid technique and tufts and flow cones were used to identify the surface streamlines, lines of separation, and regions of separated flow.

A strong vortex system was generated by the LEX. The LEX vortex core breakdown location moved forward with increasing angle of attack and fell within the scatter of similar data from ground faculties despite the wide range in Reynolds numbers.

The LEX vortex core breakdown location was also a function of angle of sideslip. For a constant angle of attack, the windward LEX vortex core breakdown location moves forward and inboard with increasing sideslip, while the leeward vortex core breakdown location moves aft and outboard.

An interaction between the forebody and LEX vortex cores occurred in which the forebody vortex core is drawn down under the LEX vortex. At 0° sideslip, this occurs just behind the LEX vortex core breakdown location.

Primary and secondary separation lines were identified on the forebody, while secondary and tertiary separation lines were observed on the LEX even after vortex core breakdown. A surprising amount of laminar flow was found on the forebody at the largest angles of attack with boundary layer transition occurring at a laminar separation bubble on the side of the fuselage despite the high Reynolds numbers. This could be explained by fact that the attachment line momentum thickness Reynolds number at the end of the laminar separation bubble is very nearly equal to the critical value.

Extensive regions of separated, reversed, and vortical flow were observed on the F-18 HARV wing at $\alpha \sim 20°$, 25°, and 30°. The influence of the LEX vortex at these angles of attack appears to keep the flow attached on the inboard portion of the wing. As the angle of attack was increased from 20° to 30°, less attached flow was observed on the inboard leading-edge flap with the separated flow advancing from outboard to inboard.

Extensive regions of unsteady and separated flow were also noted on the vertical fins when vortex core breakdown occurred forward of them. At $\alpha > 44°$, an expanding region of attached flow on the outboard surface of the fins could contribute to the increased lateral-directional control authority at these angles of attack.

REFERENCES

1. Skow, A.M.; and Erickson, G.E.: "Modern Fighter Aircraft Design for High-Angle-of-Attack Maneuvering." AGARD LS-121, paper no. 4, 1982.

2. Erickson, Gary E.: *Water Tunnel Flow Visualization and Wind Tunnel Data Analysis of the F/A-18.* NASA-CR 165859, 1982.

3. Banks, Daniel W.: "Wind-Tunnel Investigation of the Forebody Aerodynamics of a Vortex-Lift Fighter Configuration at High Angles of Attack." SAE Paper 881419, Aerospace Technology Conference and Exposition, Oct. 1988.

4. Erickson, G.E.; Hall, R.M.; Banks, D.W.; Del Frate, J.H.; Schreiner, J.A.; Hanley, R.J.; and Pulley, C.M.: "Experimental Investigation of the F/A-18 Vortex Flow at Subsonic Through Transonic Speeds, Invited Paper," AIAA 89-2222, July 1989.

5. Thomas, James L.; Walters, Robert W.; Reu, Taekyu; Ghaffari, Farhad; Weston, Robert P.; and Luckring, James M.: "A Patched-Grid Algorithm for Complex Configurations Directed Towards the F/A-18 Aircraft." AIAA 89-0121, Jan. 1989.

6. Ghaffari, F.; Luckring, J.M.; Thomas, J.L.; and Bates, B.L.: "Navier-Stokes Solutions About the F/A-18 Forebody-LEX Configuration." AIAA 89-0338, Jan. 1989.

7. Schiff, Lewis B.; Cummings, Russell M.; Sorenson, Reese L.; and Rizk, Yehia M.: "Numerical Simulation of High-Incidence Flow Over the F-18 Fuselage Forebody." AIAA 89-0339, Jan. 1989.

8. Schiff, L.B.; Cummings, R.M.; Sorenson, R.L.; and Rizk, Y.M.: "Numerical Simulation of F-18 Fuselage Forebody Flow at Large Angles of Attack." Presented at the NASA CFD Conference, Moffett Field, CA, March 7–9, 1989.

9. Cummings, Russell M.; Rizk, Yehia M.; Schiff, Lewis B.; and Chaderjian, Neal M.: "Navier-Stokes Predictions of the Flowfield Around the F-18 (HARV) Wing and Fuselage at Large Incidence." AIAA 90-0099, Jan. 1990.

10. Fisher, David F., Richwine, David M.; and Banks, Daniel W.: *Surface Flow Visualization of Separated Flows on the Forebody of an F-18 Aircraft and Wind-Tunnel Model.* NASA TM-100436, 1988. Also published as AIAA 88-2112, 1988.

11. Fisher, David F.; and Meyer, Robert R., Jr.: *Flow Visualization Techniques for Flight Research.* NASA TM-100455, 1988. Also published in *Flight Test Techniques*, AGARD CP 452, paper no. 20.

12. Fisher, D.F.; Curry, R.E.; Del Frate, J.H.; and Richwine, D.M.: "In-Flight Flow Visualization Techniques on a Vortex-Lift Fighter Aircraft." Fifth International Symposium on Flow Visualization, Prague, Czechoslovakia, August 21–25, 1989.

13. Fisher, David F.; Del Frate, John H.; and Richwine, David M.: "In-Flight Flow Visualization Characteristics of the NASA F-18 High Alpha Research Vehicle at High Angles of Attack." SAE 892222, Aerospace Technology Conference and Exhibition, Sept. 1989. Also published as NASA TM-4193, 1990.

14. Schneider, Edward T.; and Meyer, Robert R., Jr.: "F-18 High Alpha Research Vehicle: Description, Results and Plans." SETP 33rd Symposium Proceedings, Sept. 1989.

15. Del Frate, John H.; Fisher, David F.; and Zuniga, Fanny A.: "In-Flight Flow Visualization With Pressure Measurements at Low Speeds on the NASA F-18 High Alpha Research Vehicle." AGARD Vortex Flow Aerodynamics Conference, paper no. 13, Oct. 1-4, 1990. Also published as NASA TM-101726, 1990.

16. Curry, Robert E.; and Richwine, David M.: "An Airborne System for Vortex Flow Visualization on the F-18 High-Alpha Research Vehicle." AIAA 88-4671, Sept. 1988.

17. Richwine, David M.; and Curry, Robert E.: *A Smoke Generator for Aerodynamic Flight Research.* NASA TM-4137, 1989.

18. Del Frate, John H.; and Zuniga, Fanny A.: "In-Flight Flow Field Analysis on the NASA F-18 High Alpha Research Vehicle With Comparisons to Ground Facility Data." AIAA 90-0231, Jan. 1990.

19. Fisher, David F.; Banks, Daniel W.; and Richwine, David M.: "F-18 High Alpha Research Vehicle Surface Pressures: Initial In-Flight Results and Correlation With Flow Visualization and Wind Tunnel Data." AIAA 90-3018, Aug. 1990. Also published as NASA TM-101724, 1990.

20. Whitmore, Stephen A.; Moes, Timothy R.; and Larson, Terry J.: "Preliminary Results From a Subsonic High Angle-of-Attack Flush Airdata Sensing (HI-FADS) System: Design, Calibration, and Flight Test Evaluation." NASA TM-101713, 1990. Also published as AIAA 90-0232, Jan. 1990.

12

21. Fennell, L.J.: "Vortex Breakdown—Some Observations in Flight on the HP-115 Aircraft." Reports and Memoranda No. 3805, Sept. 1971. Replaces R.A.E. Technical Report 71177 - A.R.C. 34 400.

22. Belevtsov, N.; Brumby, R.E.; and Hughes, J.P.: "In-Flight Flow Visualization, A Fluid Approach." SFTE, 14th Annual Symposium Proceedings, Aug. 1983, pp. 4.2-1 to 4.2-7.

23. Crowder, J.P.: "Flow Visualization In Flight Testing." AIAA 90-1273, May 1990.

24. Bisgood, P.L.: *The Application of a Surface Flow-Visualization Technique in Flight*, Reports and Memoranda No. 3769, Feb. 1974. Replaces R.A.E. Technical Report 74022 - A.R.C. 35 554.

25. Meyer, R.R., Jr.; and Schneider, E.T.: "Real-Time Pilot Guidance System for Improved Flight Test Maneuvers." AIAA 83-2747, Nov. 1983. Also published as NASA TM-84922, 1984.

26. Frazier, F. Allen: "F-18 Hornet - LEX Fence Flight Test Results." SETP 32nd Symposium Proceedings, Oct. 1988.

27. Werle, H.: "Flow Visualization Techniques for the Study of High Incidence Aerodynamics," AGARD–VKI lecture series 121, 1982.

28. Lee, B.H.K.; Brown, D.; Zgela, M.; and Poirel, D.: "Wind Tunnel Investigation and Flight Tests of Tail Buffet on the CF-18 Aircraft." AGARD Structures and Materials Panel 70th Meeting, Sorrento (Naples), Italy, April 1–6, 1990.

29. Behel, Ivan M.; and McNamara, William G.: "F/A-18A High Angle of Attack/Spin Testing." SETP 25th Symposium Proceedings, Sept. 1981.

30. Polhamus, Edward C.: "A Review of Some Reynolds Number Effects Related to Bodies at High Angles of Attack." NASA CR-3809, 1984.

31. Poll, D.I.A.: "Leading Edge Transition on Swept Wings." AGARD CP-224, paper no. 21, 1977.

32. Phenninger, Werner: "Laminar Flow Control, Laminarization." AGARD report no. 654, paper no. 3, 1977.
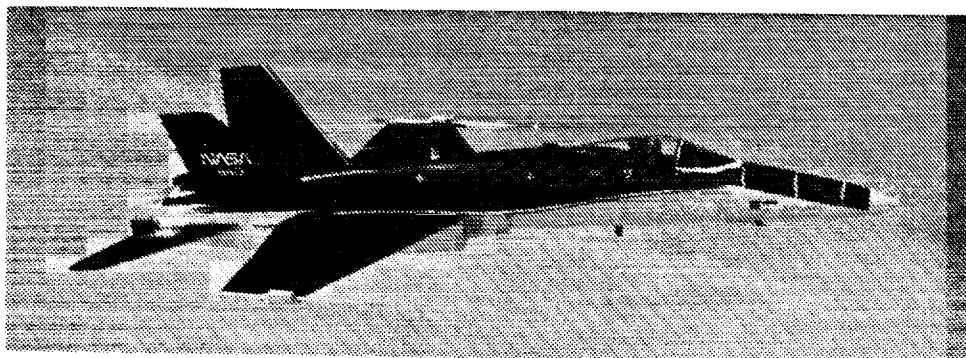
EC89 0062-001

Figure 1. The F-18 HARV.
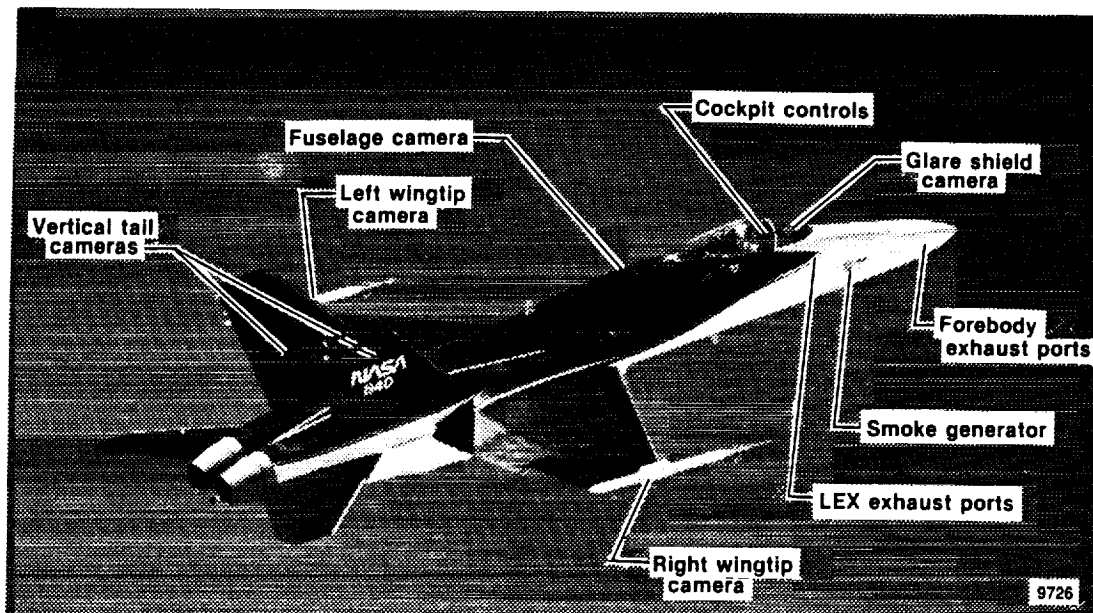
Figure 2. Locations of onboard cameras and smoke generator system on the F-18 HARV.

ORIGINAL PAGE
BLACK AND WHITE PHOTOGRAPH
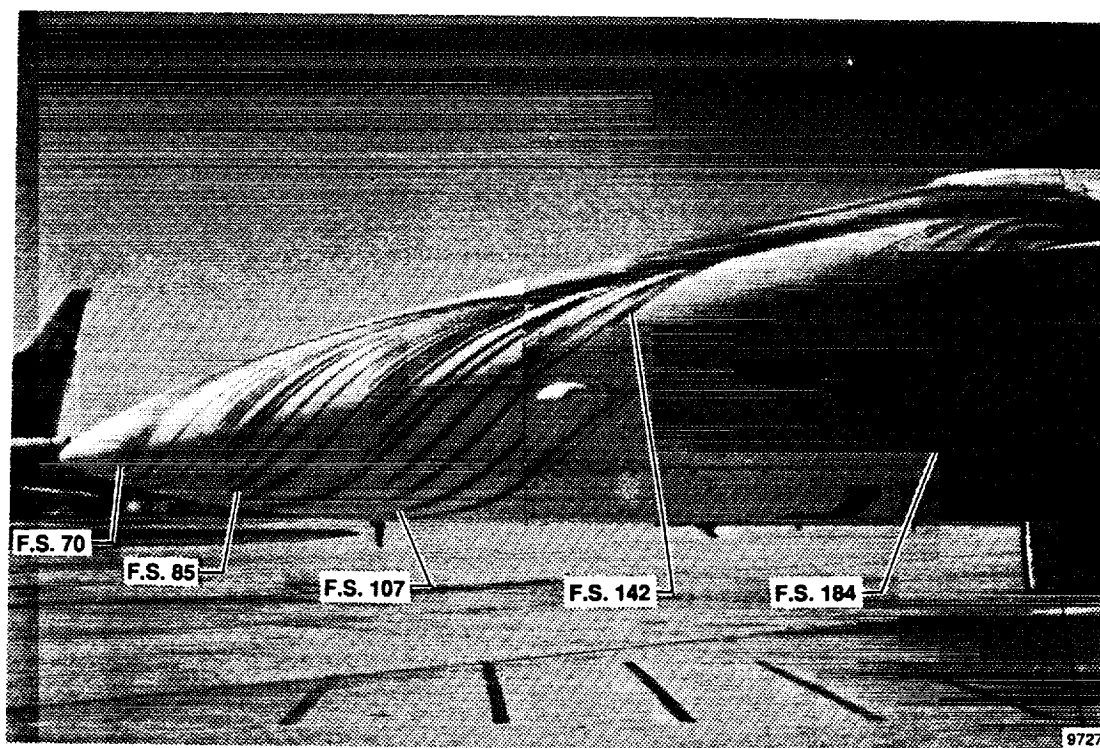
(a) Forebody locations.

Figure 3. Locations of flush surface-static orifices on the F-18 HARV.

14
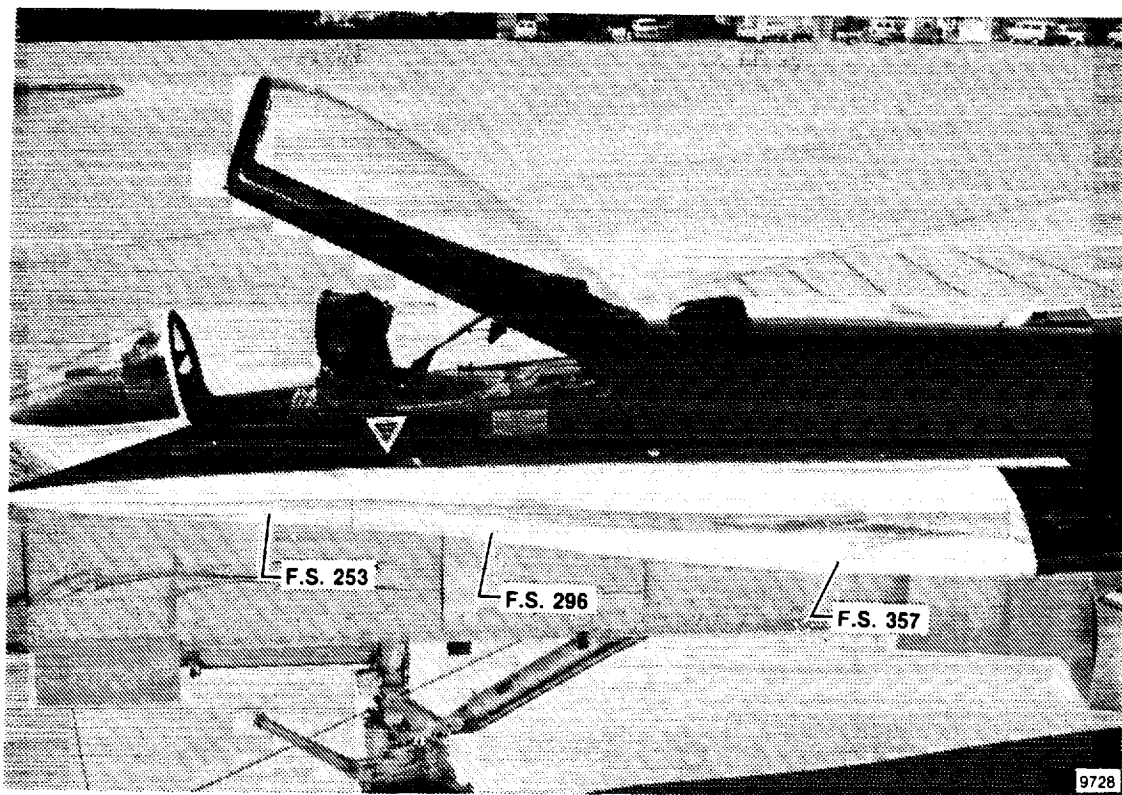
(b) LEX locations.

Figure 3. Concluded.

$\alpha = 35°$
$\beta = 0°$
$Re_{\bar{c}} = 5.5 \times 10^3$
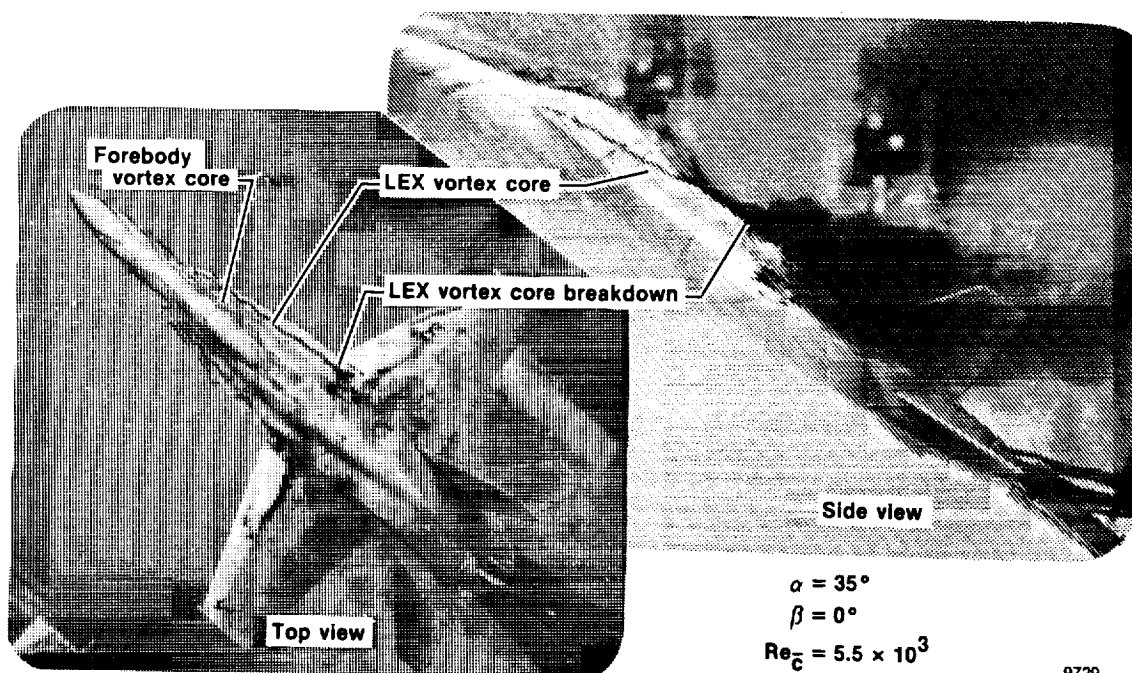
Figure 4. Vortex flow on 1/48-scale model of the F-18 HARV in the Ames-Dryden water tunnel, $\alpha = 35°$.

15
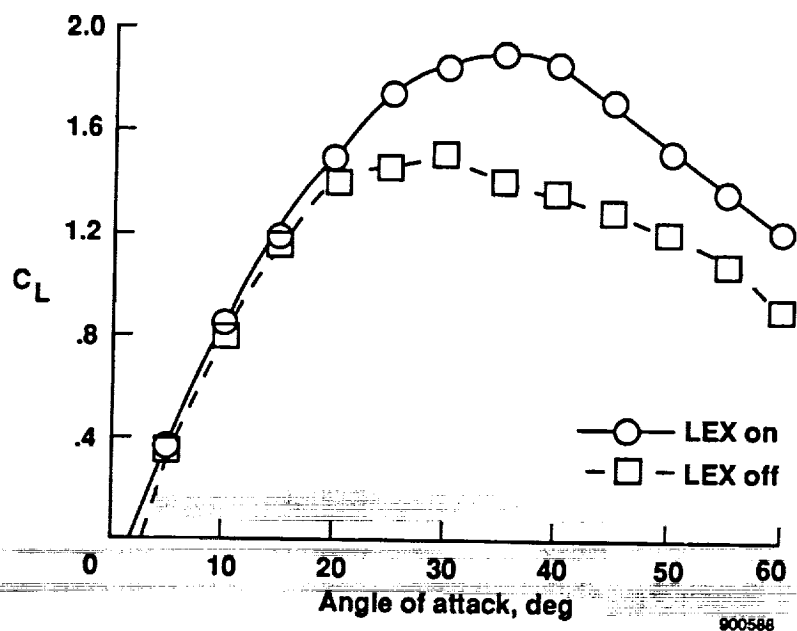
Figure 5. Wing leading-edge extension (LEX) increase of maximum lift (ref. 26).
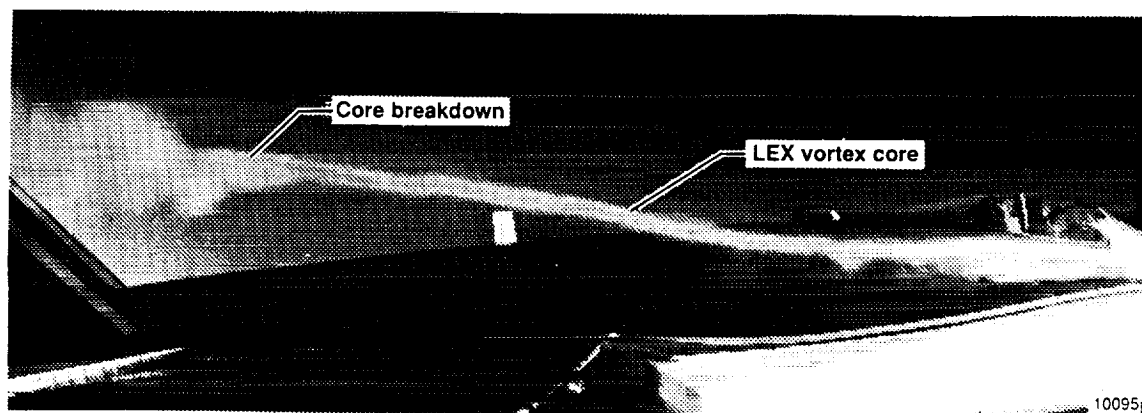
(a) $\alpha = 20.0°$ and $\beta = 0.0°$.
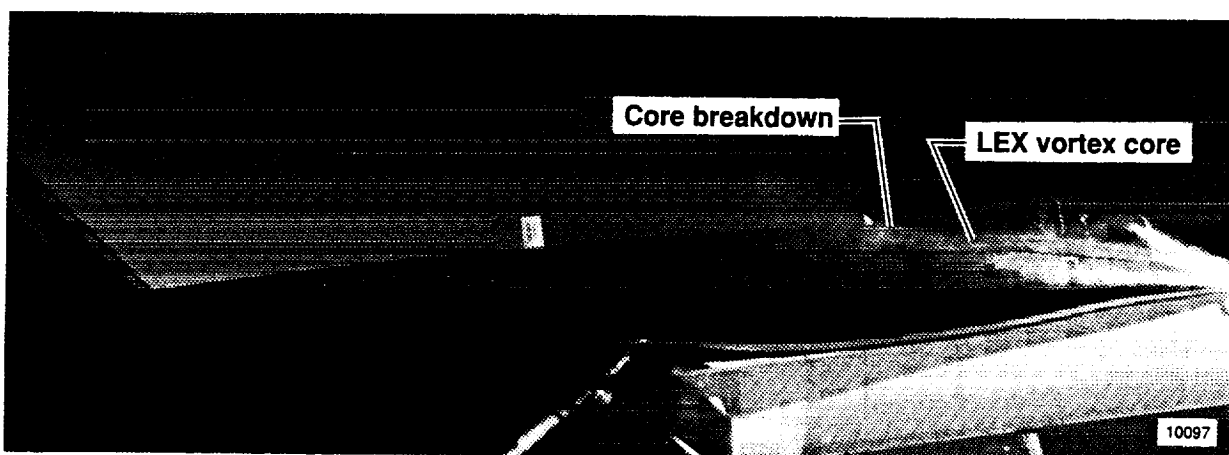
(b) $\alpha = 29.8°$ and $\beta = 0.2°$.
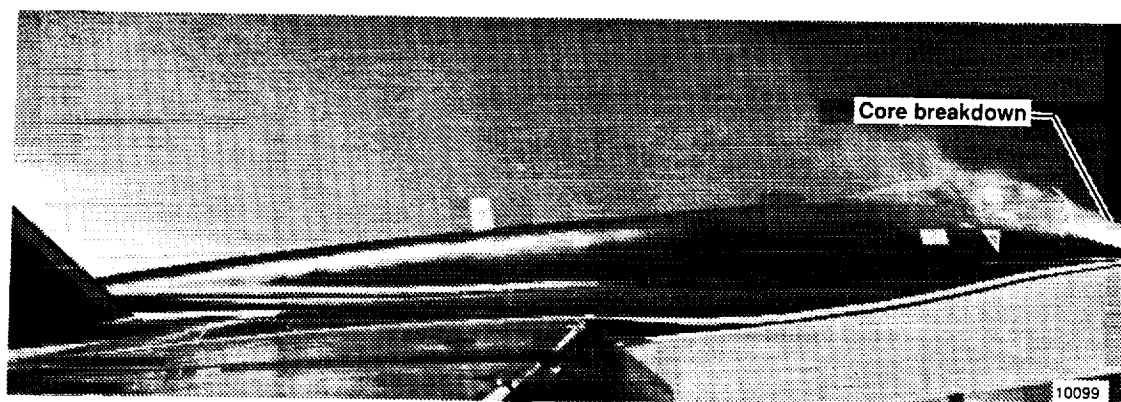
(c) $\alpha = 42.5°$ and $\beta = 0.8°$.

Figure 6. Right wingtip view of smoke flow visualization on the F-18 HARV LEX.

		$\mathrm{Re}\,\bar{c}$	Model scale, percent	Fluid medium	Ref.
●	Flight	8 to 13 x 10^6	–	Air	18
☐	DTRC	1.75 x 10^6	6	Air	4,18
◇	BART	1.60 x 10^5	3	Air	18
△	LSWT	3.60 x 10^5	12	Air	18
▽	FVF	1.26 x 10^4	3	Water	18
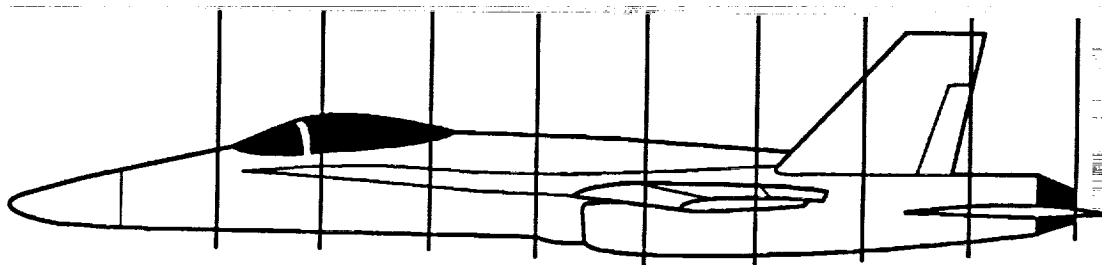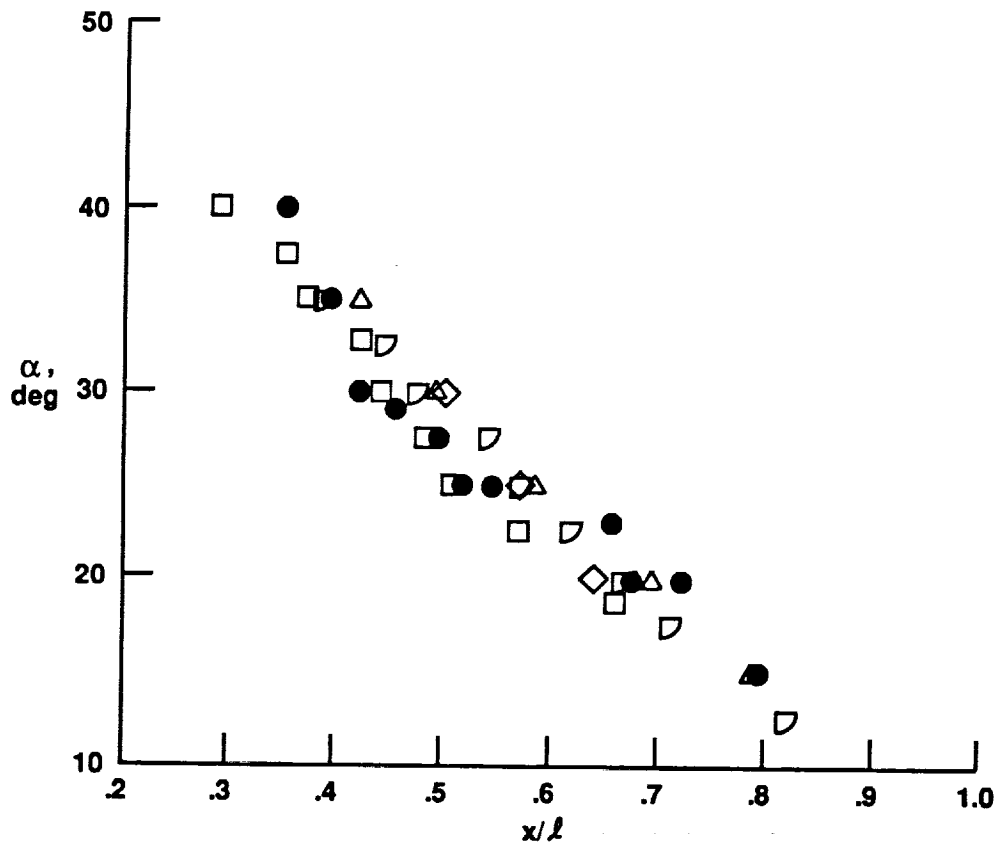
900434

Figure 7. Comparison of F-18 LEX vortex core breakdown location from flight and ground facilities.
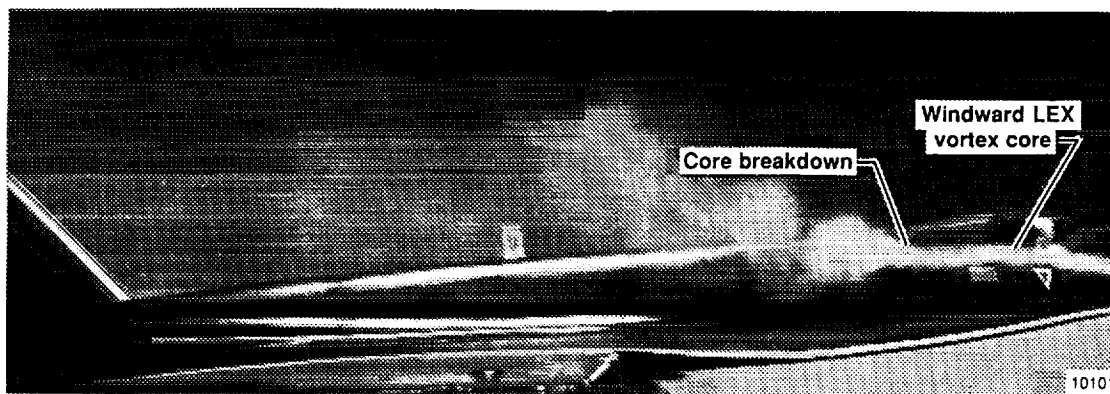
(a) $\alpha = 26°$ and $\beta = 4.5°$.
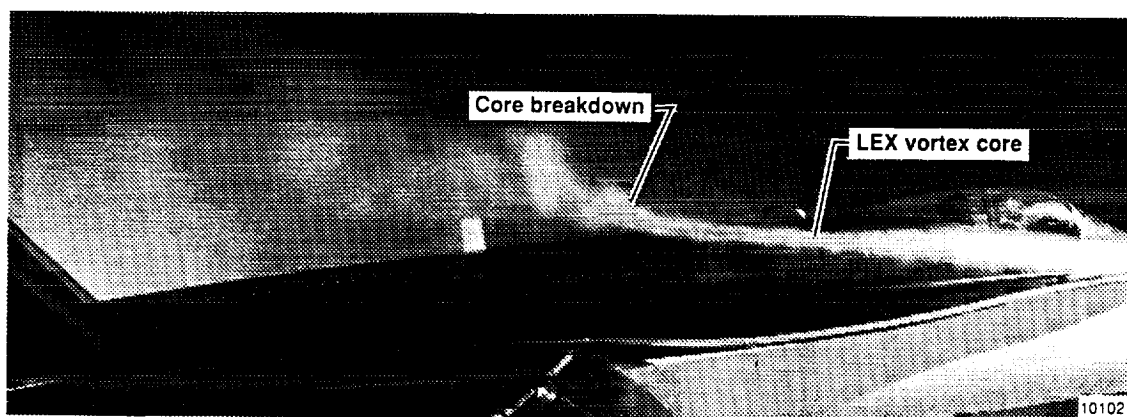
(b) $\alpha = 25°$ and $\beta = 1°$.
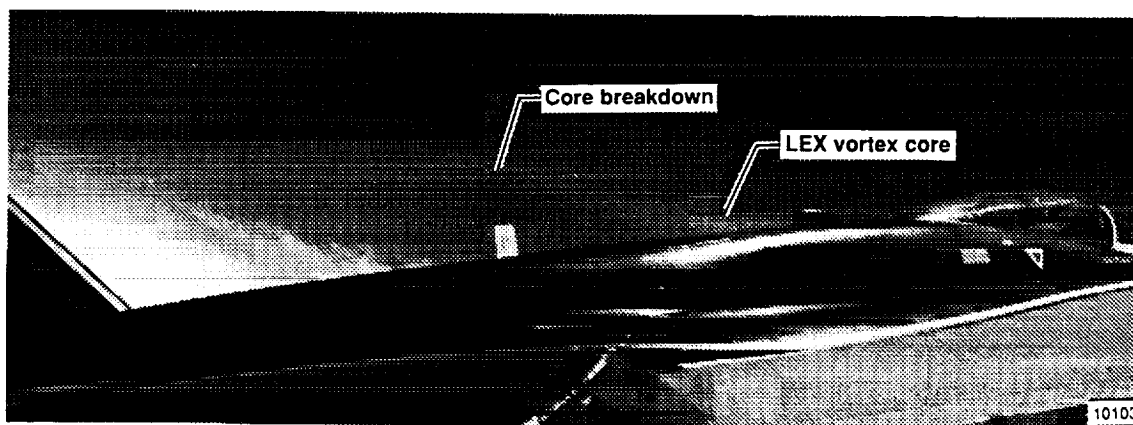
(c) $\alpha = 24.7°$ and $\beta = -3.4°$.

Figure 8. Right wingtip view showing effects of increased angle of sideslip on LEX vortex core and break-down point.
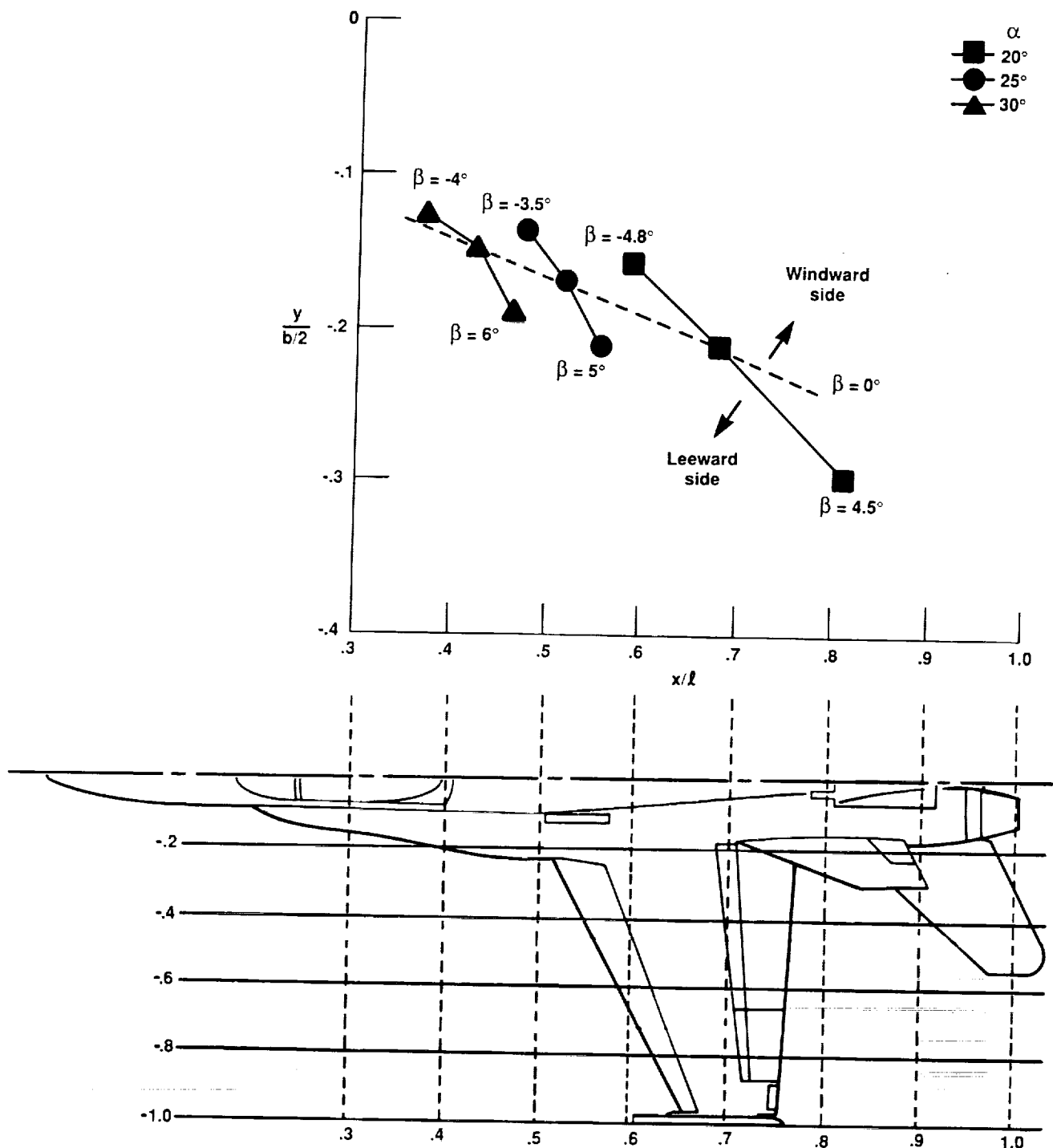
Figure 9. Comparison of left F-18 LEX vortex core breakdown location as a function of sideslip and angle of attack.

20
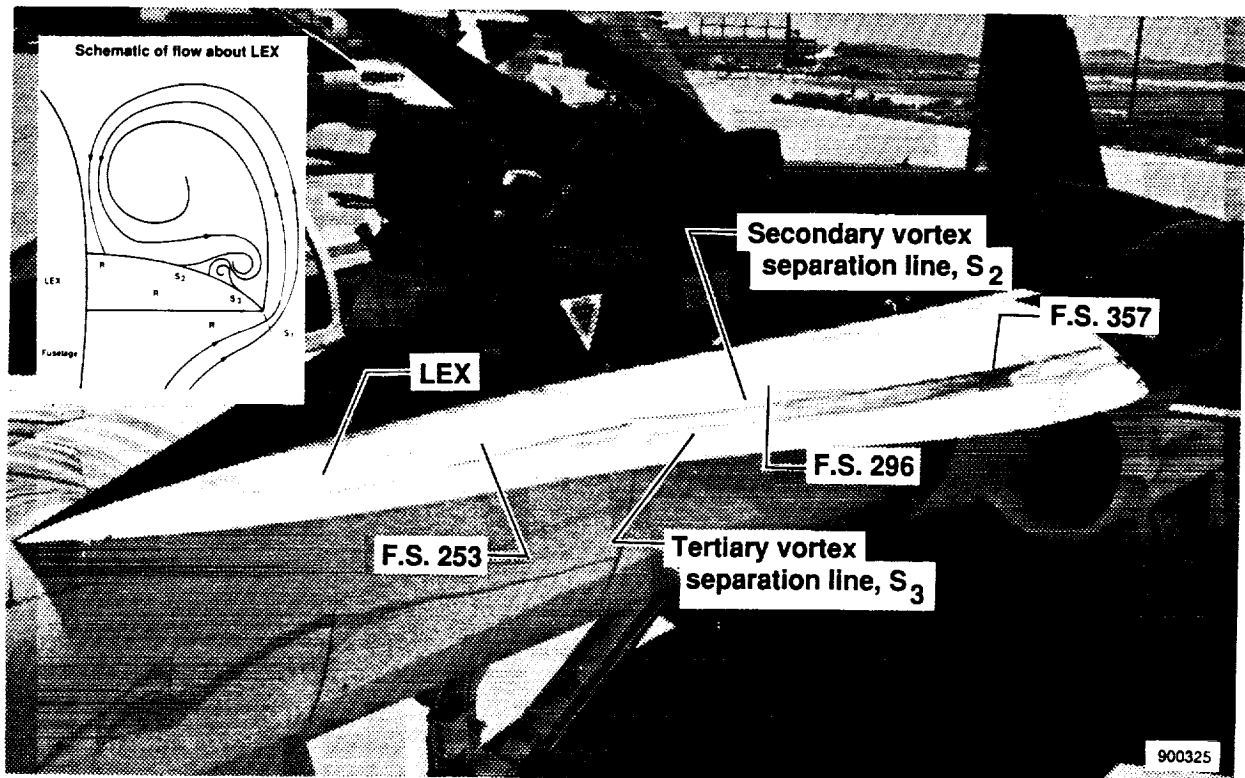
(a) $\alpha \sim 30°$.
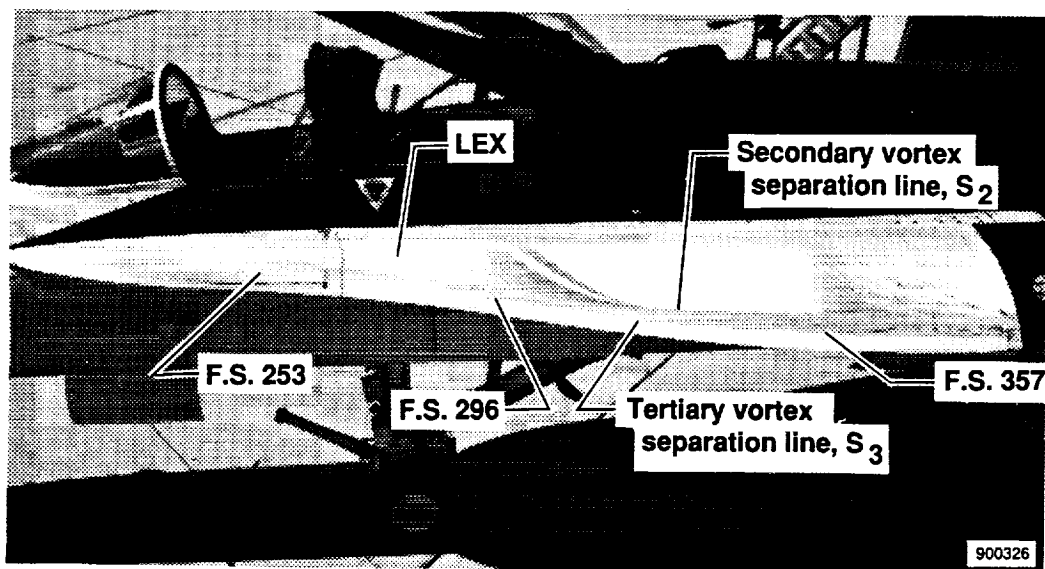
(b) $\alpha \sim 47°$.

Figure 10. Surface flow visualization on left LEX of the F-18 HARV.

(a) View from chase aircraft, $\alpha \sim 20°$.

Figure 11. Surface flow visualization on right wing of the F-18 HARV using flow tufts and cones, $\alpha \sim 20°$.
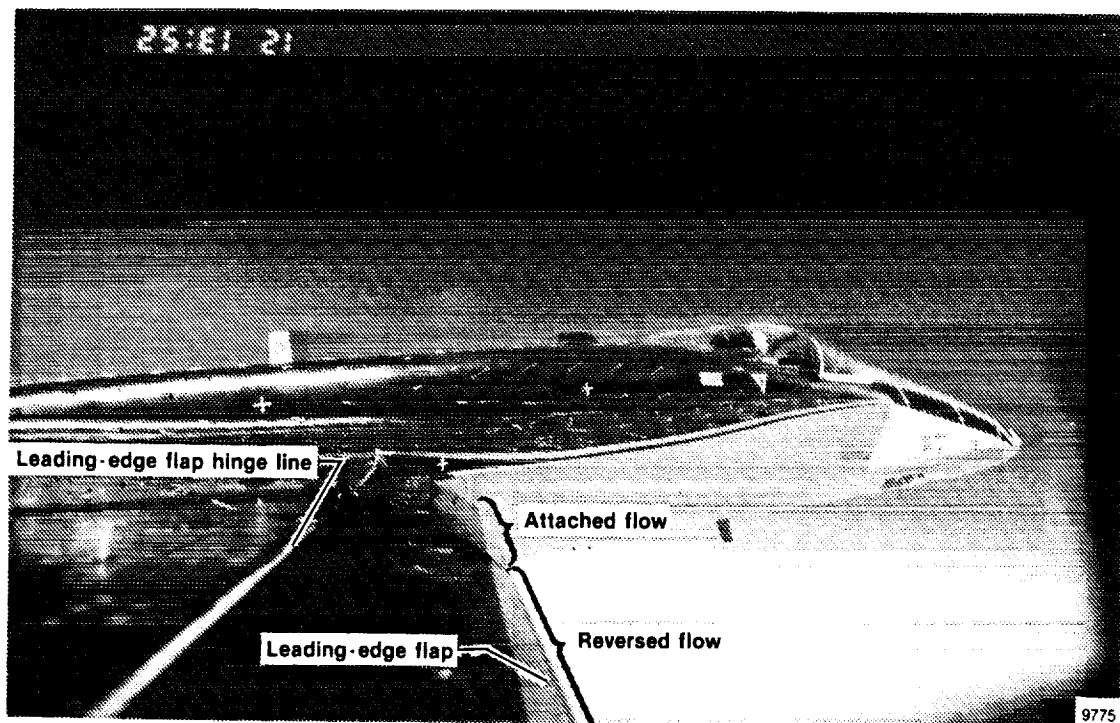
(b) Leading-edge flap, $\alpha = 19.2°$.

Figure 11. Concluded.

(a) View from chase aircraft, $\alpha \sim 25°$.

Figure 12. Surface flow visualization on right wing of F-18 HARV using flow tufts and cones, $\alpha \sim 25°$.
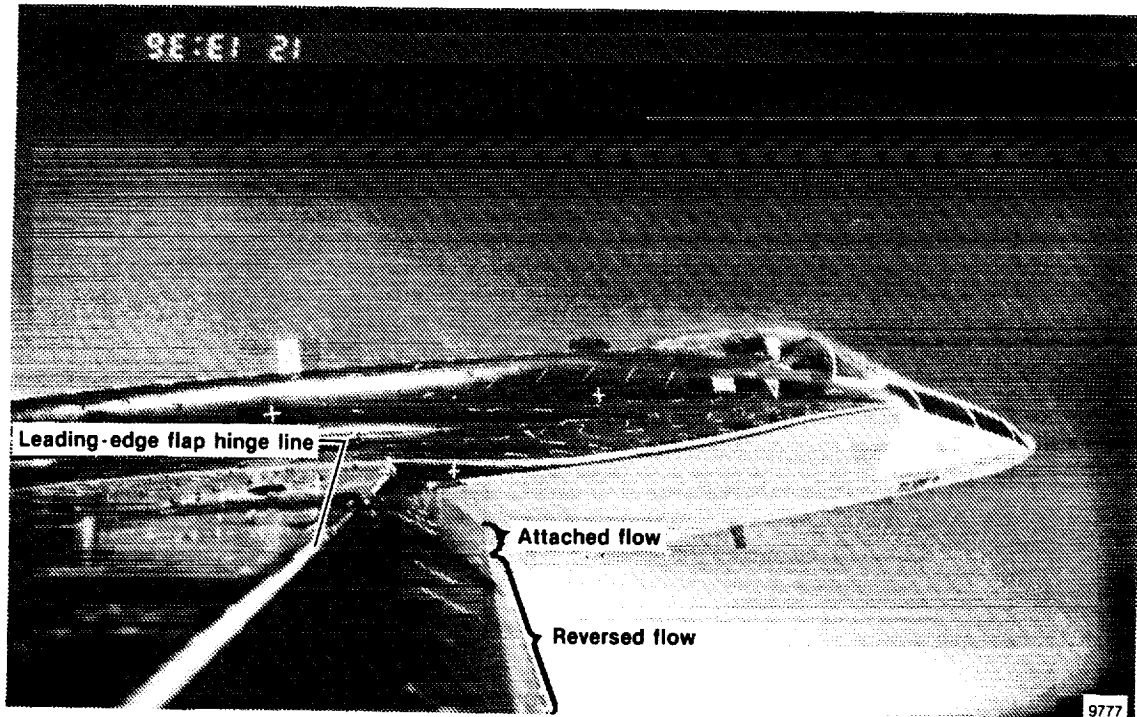
(b) Leading-edge flap, $\alpha = 24.3°$.

Figure 12. Concluded.

(a) View from chase aircraft, $\alpha \sim 30°$.

Figure 13. Surface flow visualization on right wing of F-18 HARV using flow tufts and cones, $\alpha \sim 30°$.
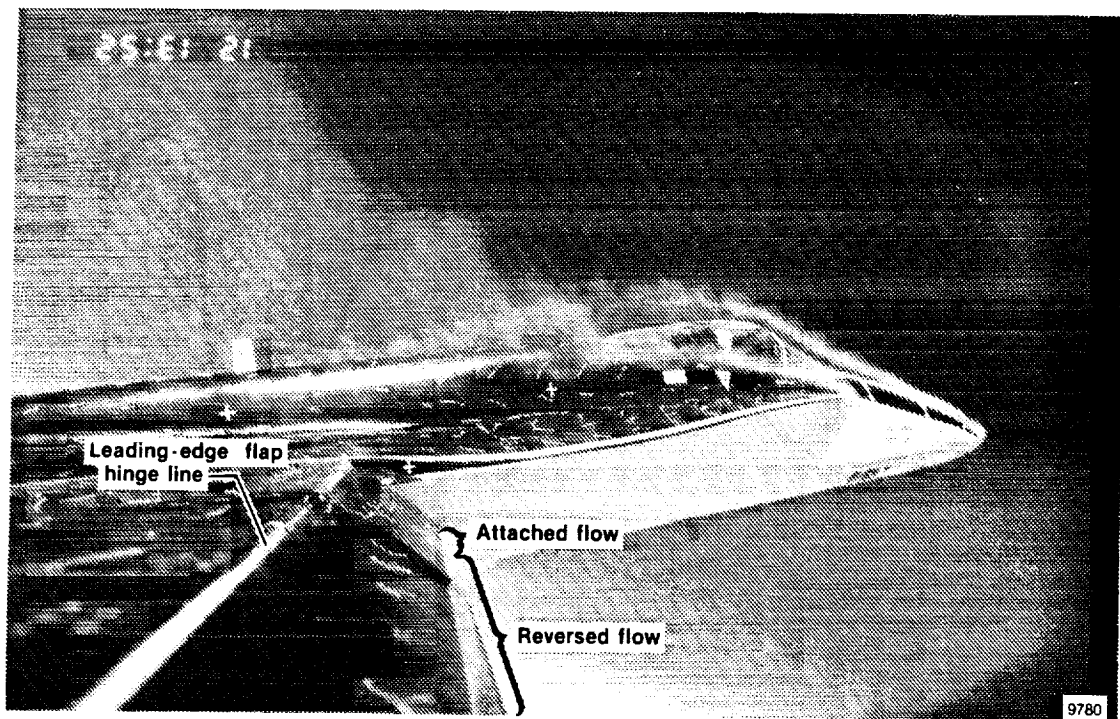
(b) Leading-edge flap, $\alpha = 31.7°$.

Figure 13. Concluded.
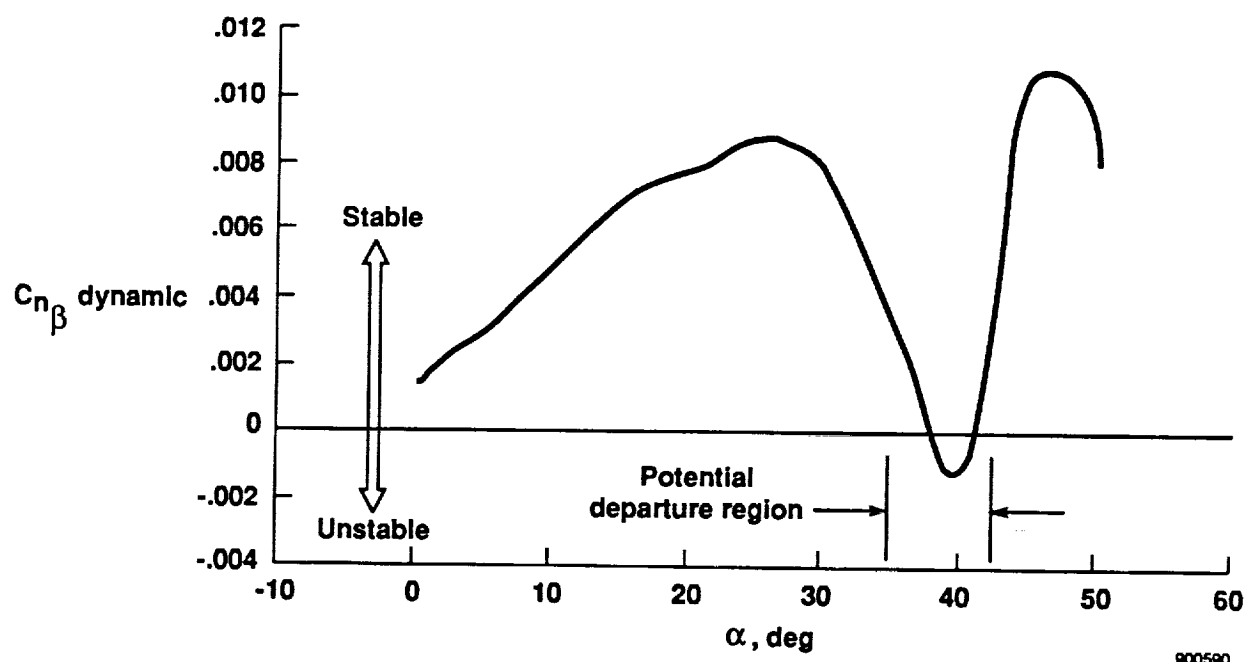
Figure 14. Directional divergence parameter as a function of angle of attack.

EC 90 0006-020

(a) $\alpha = 10°$.

EC 90 0007-019

(b) $\alpha = 30°$.

Figure 15. Tufts on he outboard surface of the right vertical stabilizer.

29
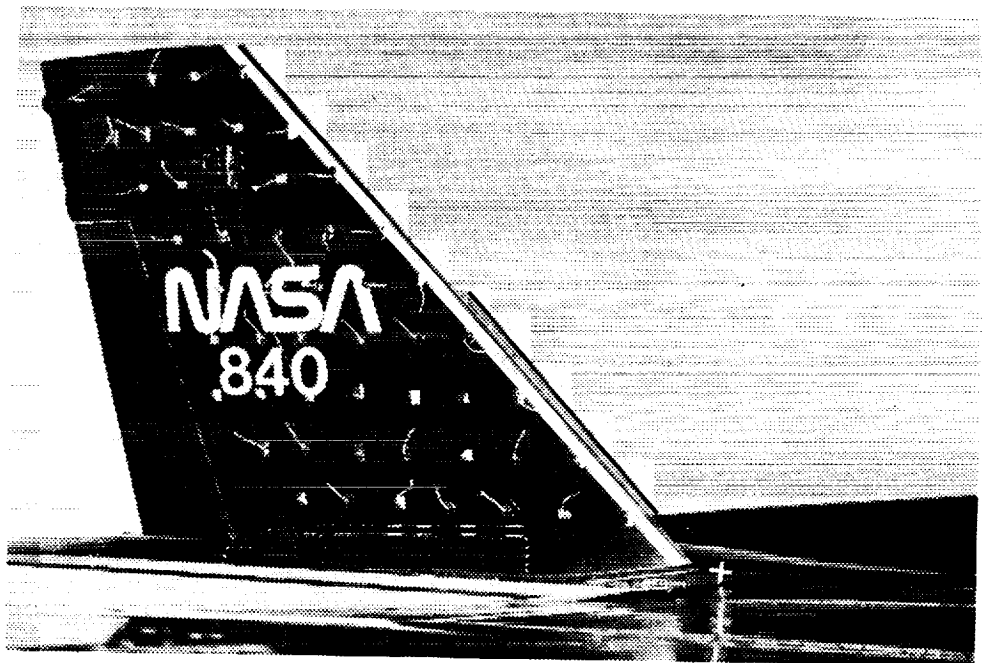
EC 90 0007-056

(c) $\alpha = 50°$.

Figure 15. Concluded.

(a) $\alpha \sim 10°$.

(b) $\alpha \sim 20°$.
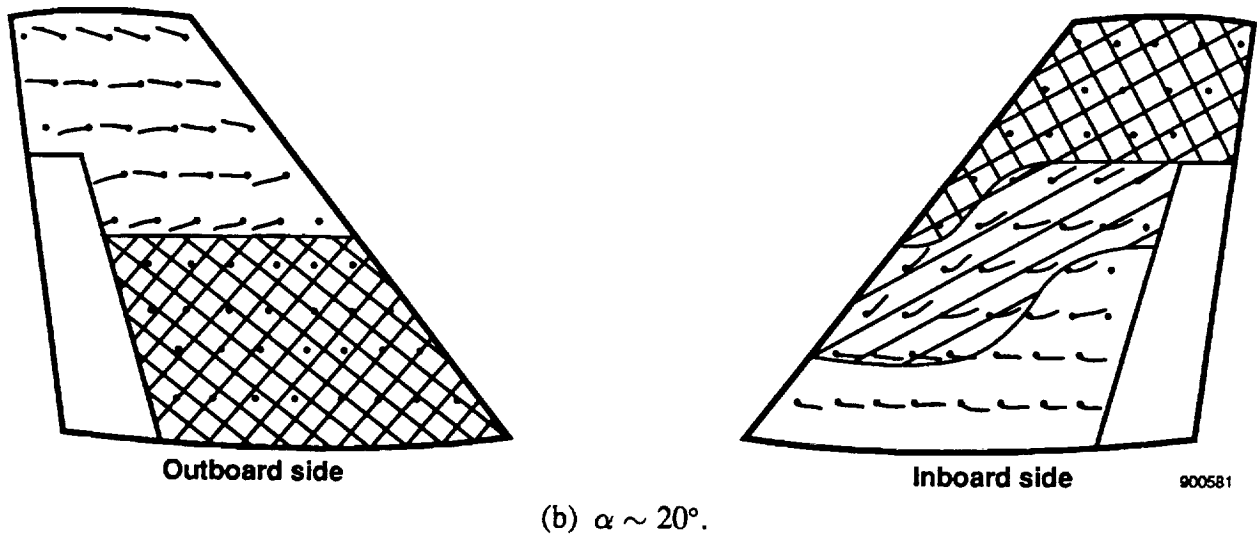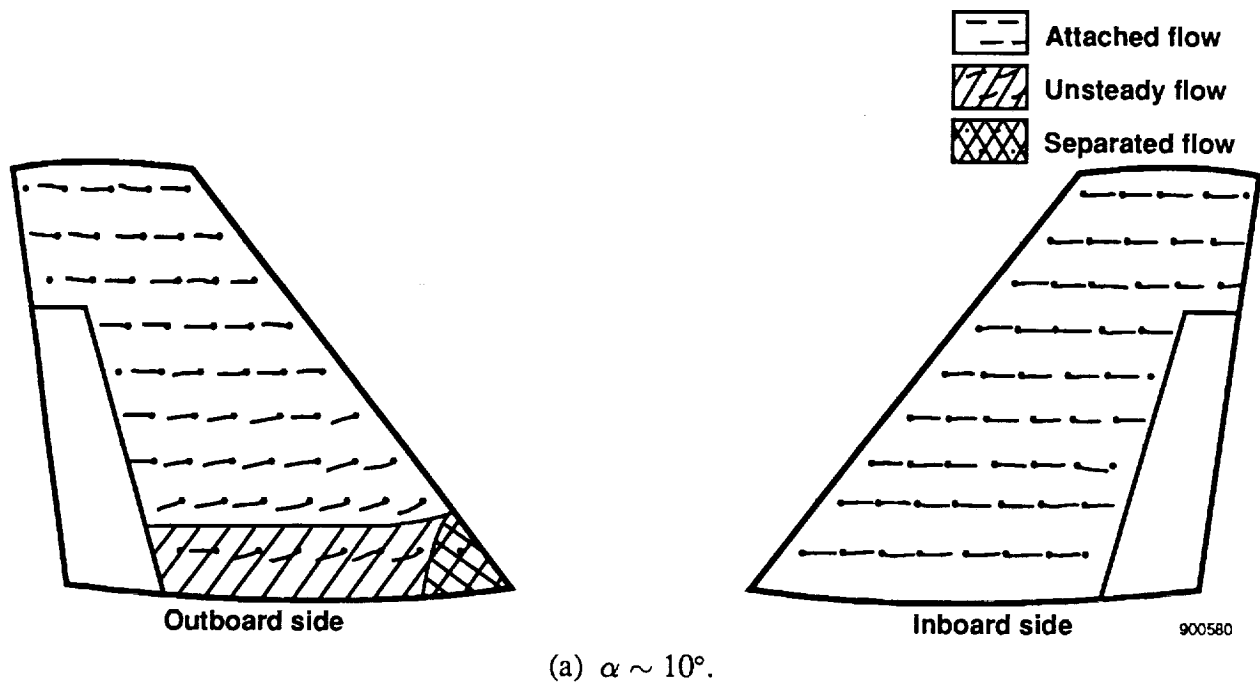
Figure 16. Interpretation of flow on vertical stabilizers from tuft observations.

31

Attached flow
Unsteady flow
Separated flow

Outboard side

Inboard side

900582

(c) $\alpha \sim 25°$.

Outboard side

Inboard side

900583

(d) $\alpha \sim 30°$.

Figure 16. Continued.

32

Attached flow

Unsteady flow

Separated flow

(e) $\alpha \sim 37°$.

900584

(f) $\alpha \sim 44°$.

900585

(g) $\alpha \sim 46°$.

900586

(h) $\alpha \sim 50°$.

900587

Outboard side
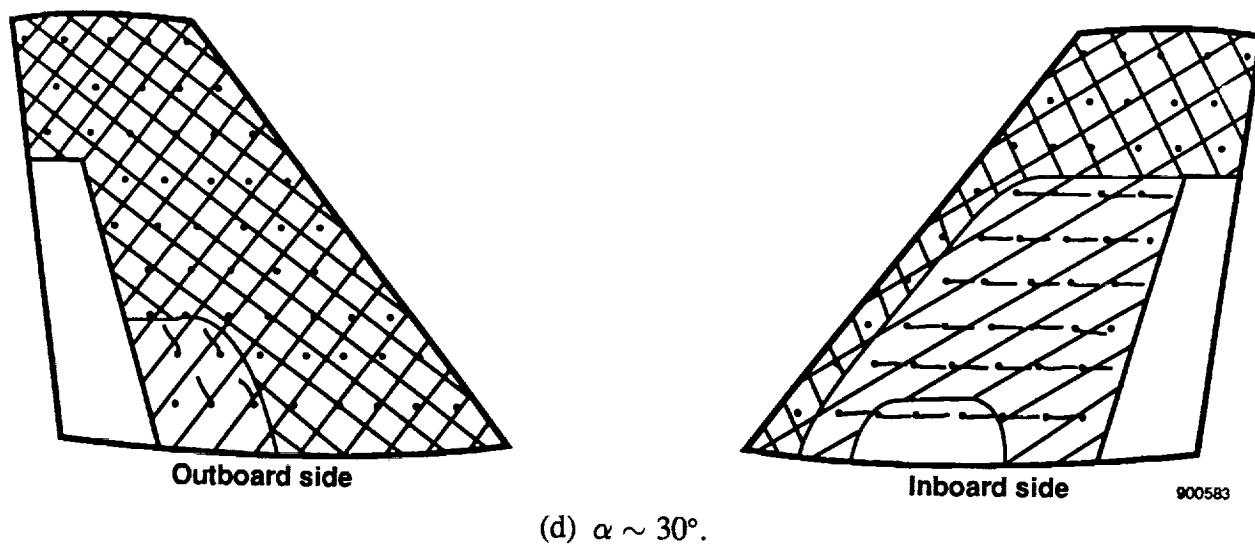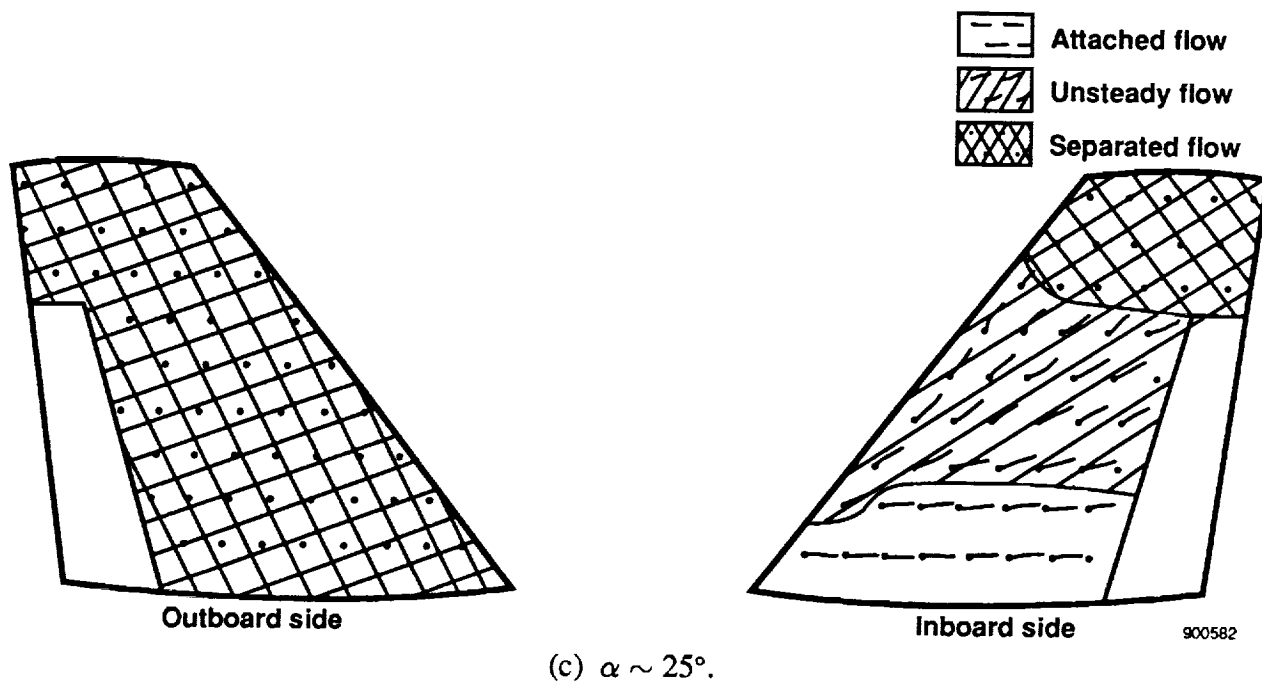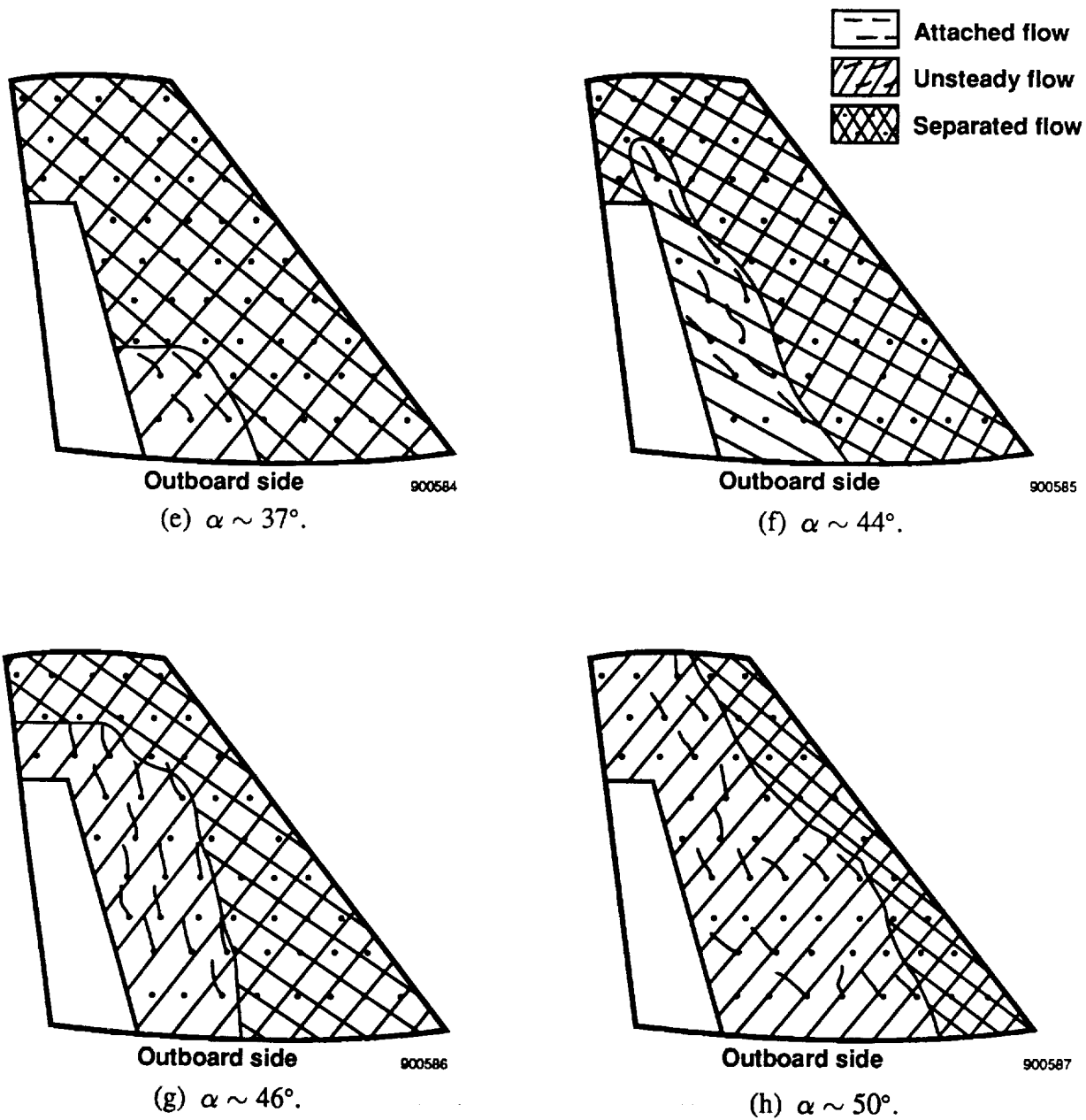
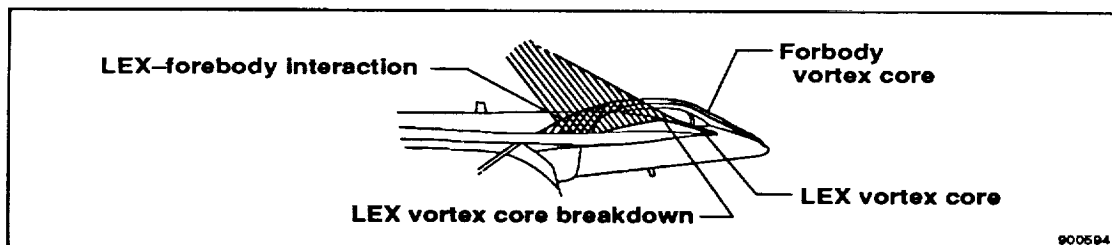Figure 16. Concluded.
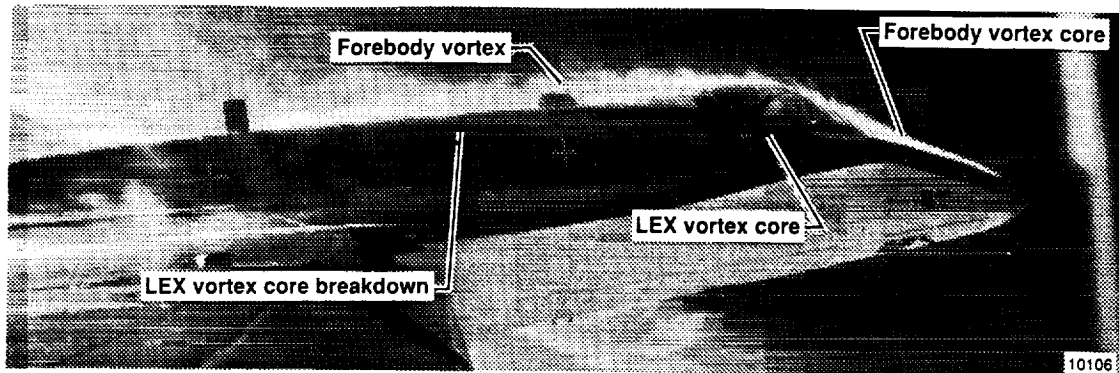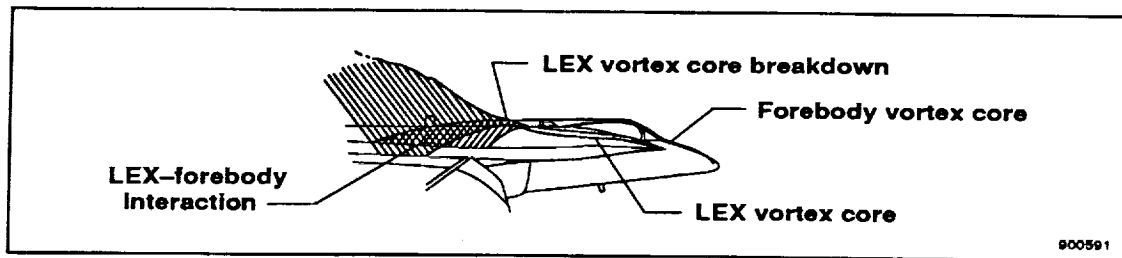
(a) $\alpha = 25.3°$ and $\beta = 0.7°$.
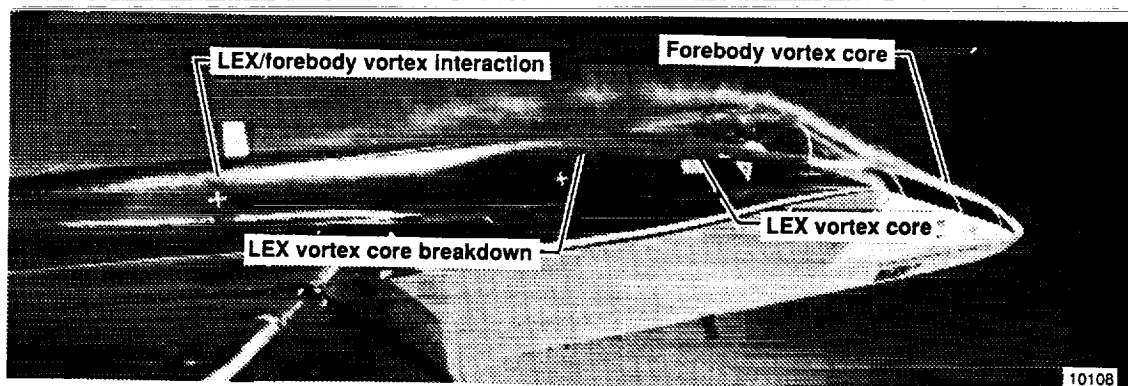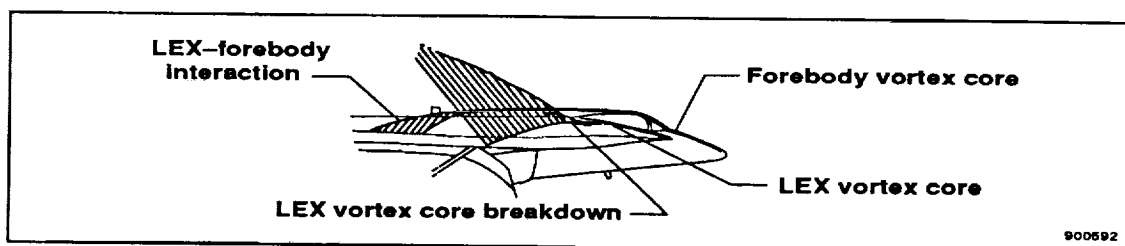
(b) $\alpha = 29.5°$ and $\beta = 0.4°$.
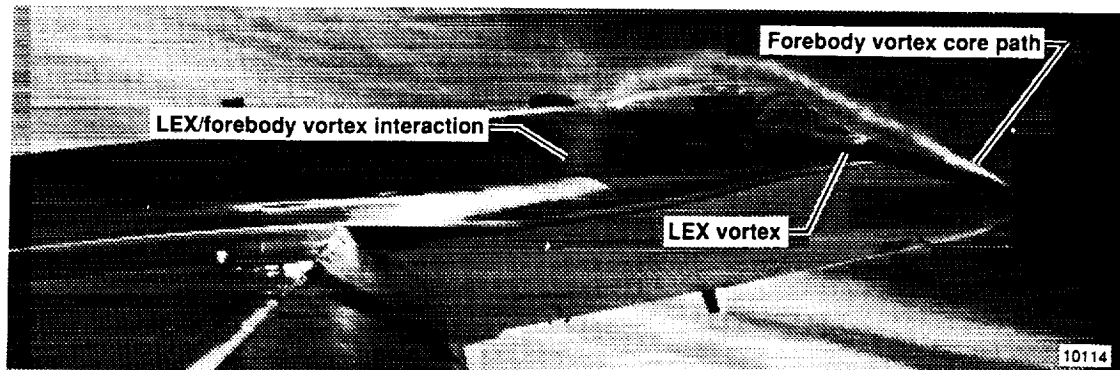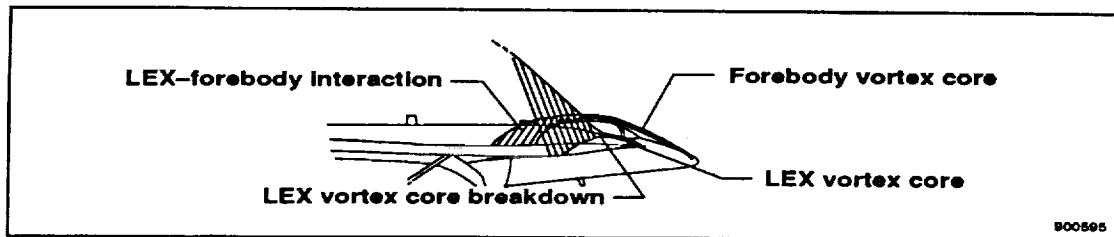
Figure 17. Wingtip view of forebody vortex system.
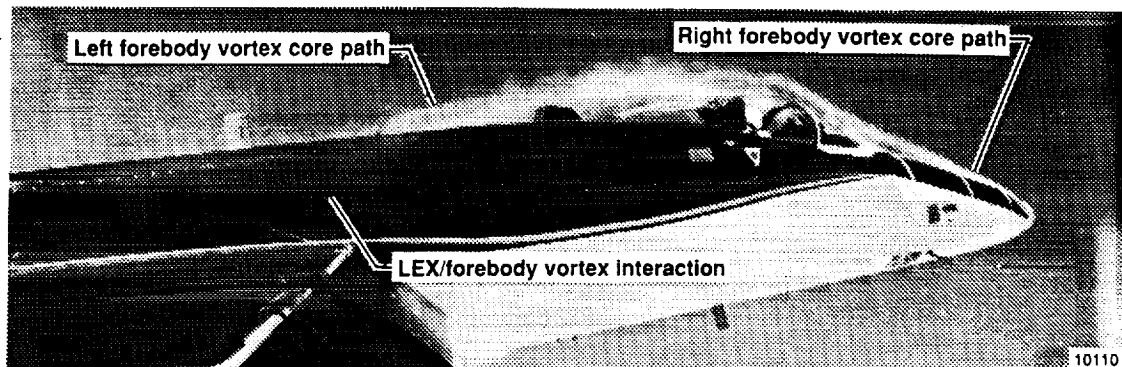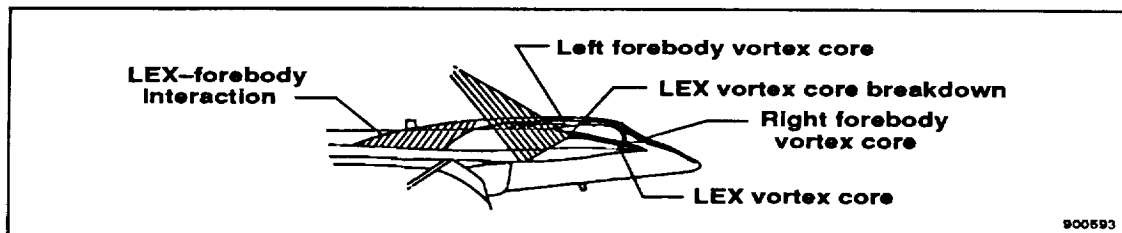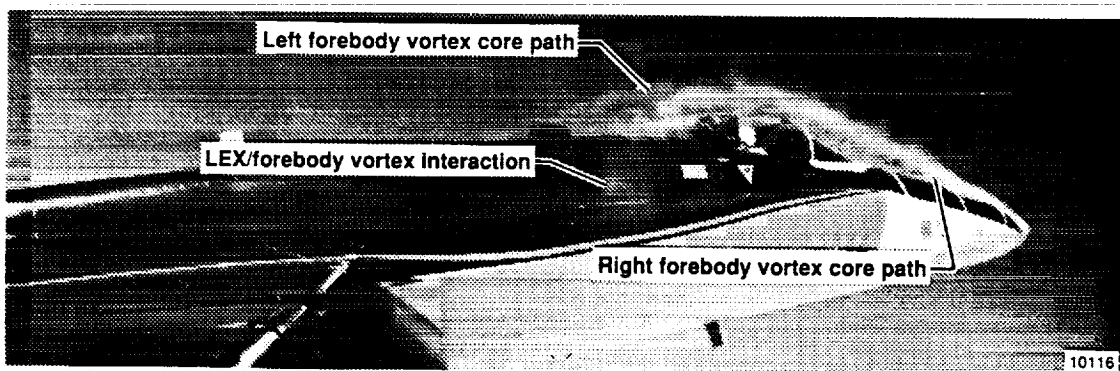
(c) $\alpha = 33.5°$ and $\beta = 0.7°$.
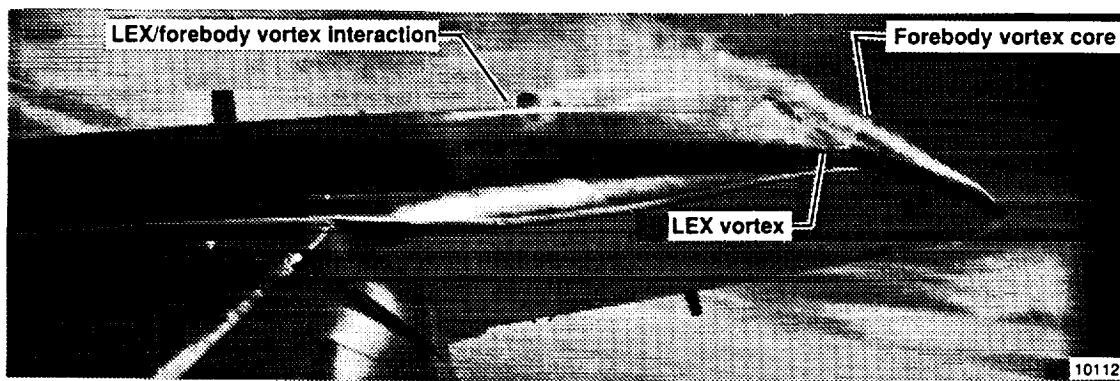
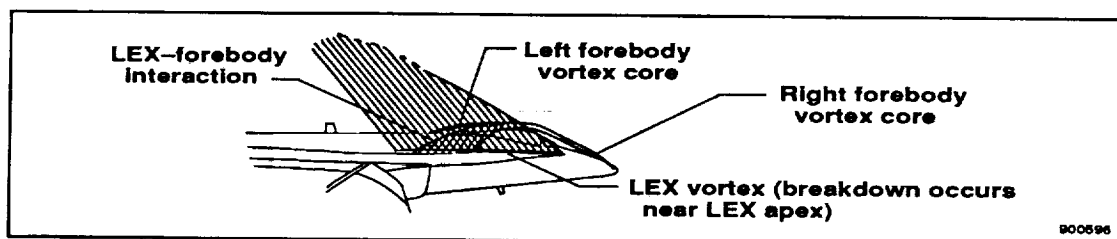(d) $\alpha = 38.7°$ and $\beta = 0°$.

Figure 17. Continued.

LEX–forebody interaction ─── Forebody vortex core

LEX vortex core breakdown ─── LEX vortex core

900595

Forebody vortex core path

LEX/forebody vortex interaction

LEX vortex

10114

(e) $\alpha = 40.6°$ and $\beta = 0.6°$.

LEX–forebody interaction ─── Left forebody vortex core

Right forebody vortex core

LEX vortex (breakdown occurs near LEX apex)

900596

Left forebody vortex core path

LEX/forebody vortex interaction

Right forebody vortex core path

10116

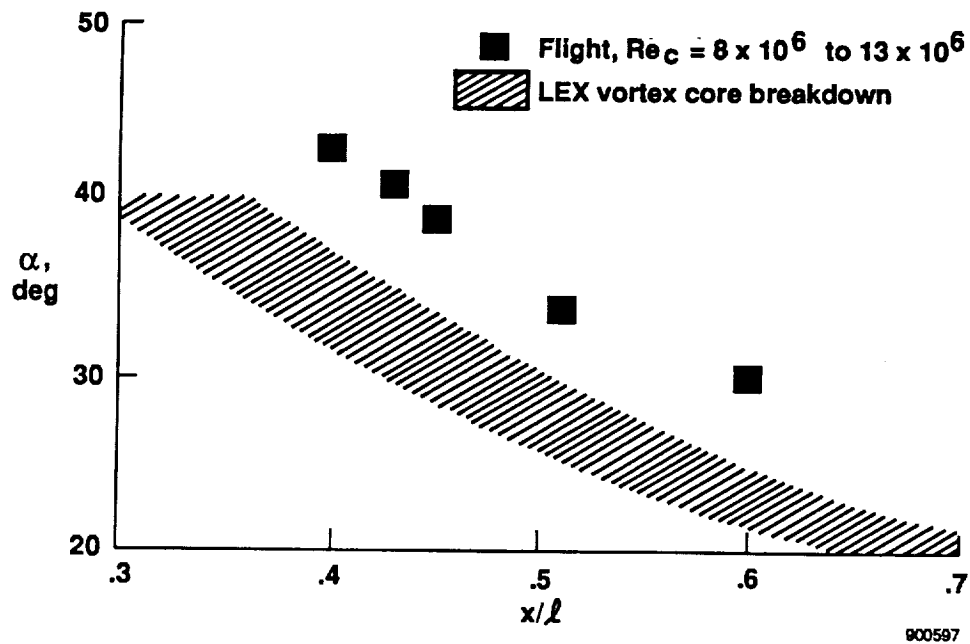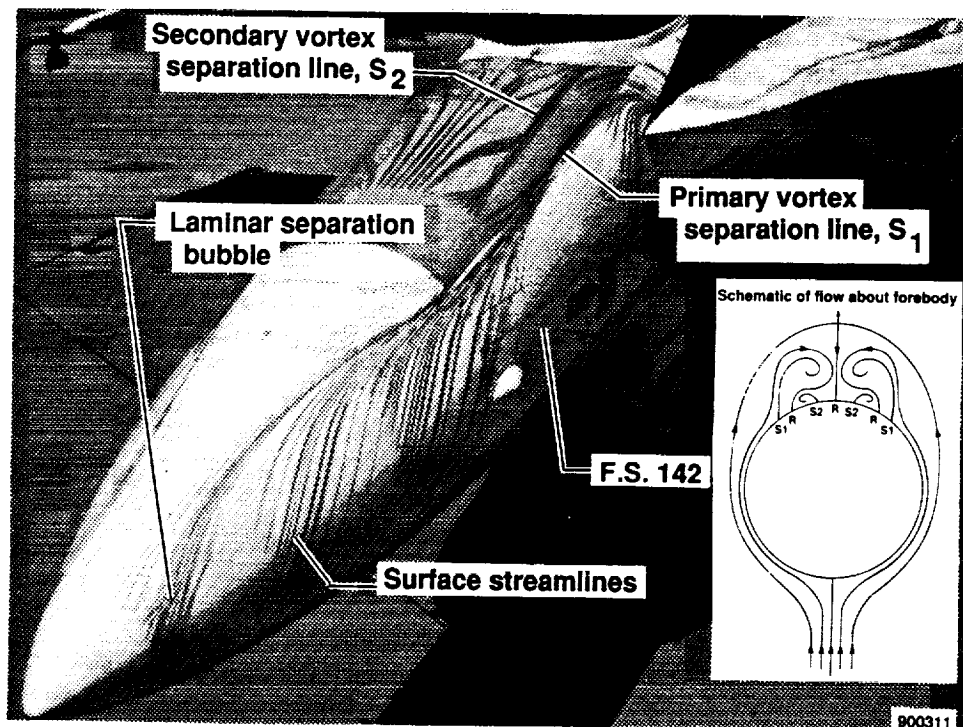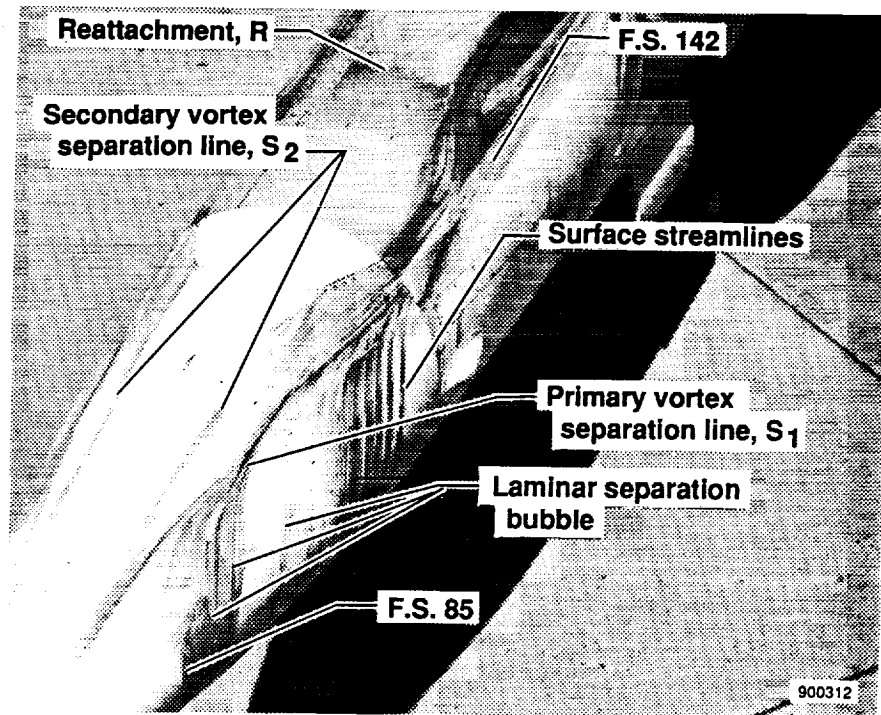(f) $\alpha = 42.5°$ and $\beta = -0.5°$.

Figure 17. Concluded.

Figure 18. Location of LEX–forebody interaction and LEX vortex core breakdown as a function of angle of attack at $\beta = 0°$.
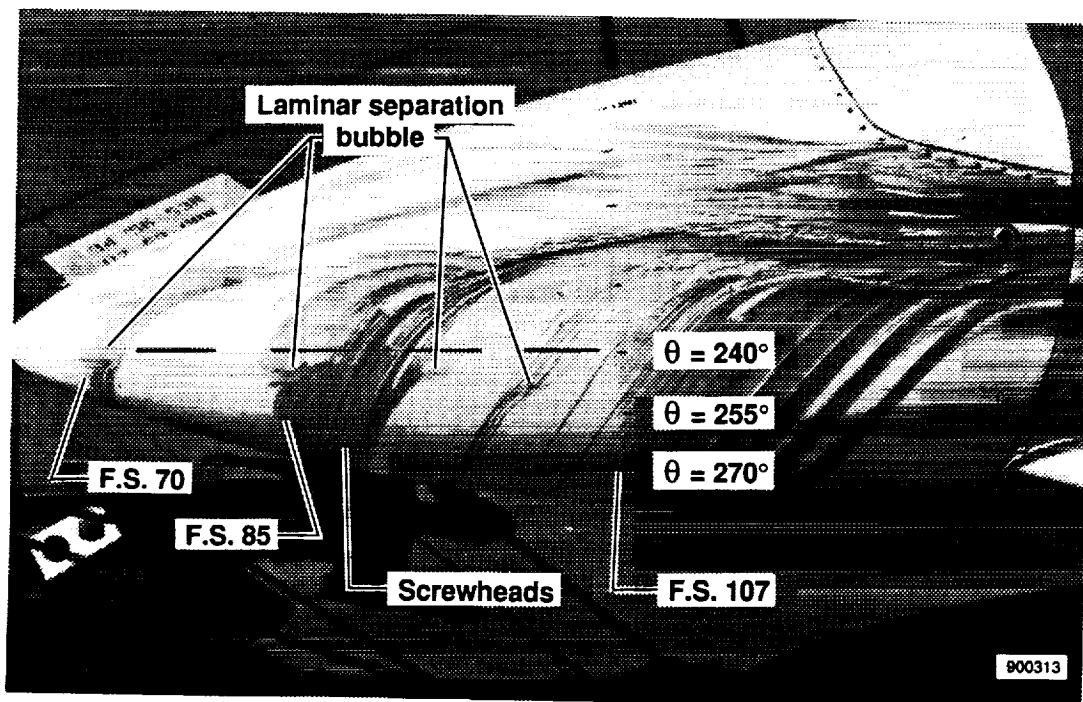

(a) $\alpha \sim 30°$.

Figure 19. Surface flow visualization on F-18 HARV forebody.

(b) 1/4 view, $\alpha \sim 47°$.

(c) Close up of nosecone, $\alpha \sim 47°$.

Figure 19. Concluded.

38

NASA

National Aeronautics and
Space Administration

Report Documentation Page

1. Report No. NASA TM-101734	2. Government Accession No.	3. Recipient's Catalog No.

4. Title and Subtitle	5. Report Date
Summary of In-Flight Flow Visualization Obtained From the NASA High Alpha Research Vehicle	January 1991
	6. Performing Organization Code

7. Author(s)	8. Performing Organization Report No.
David F. Fisher, John H. Del Frate, and Fanny A. Zuniga	H-1686
	10. Work Unit No. RTOP 505-68-71

9. Performing Organization Name and Address	
Dryden Flight Research Facility P.O. Box 273, Edwards, California 93523-0273	11. Contract or Grant No.

	13. Type of Report and Period Covered Technical Memorandum
12. Sponsoring Agency Name and Address National Aeronautics and Space Administration Washington, DC 20546-3191	
	14. Sponsoring Agency Code

15. Supplementary Notes

Presented at the High Angle of Attack Technology Symposium, Hampton, Virginia, October 30 – November 1, 1990.

16. Abstract

A summary of the surface and off-surface flow visualization results obtained in flight on the F-18 high alpha research vehicle (HARV) is presented, highlighting the extensive three-dimensional vortical flow on the aircraft at angles of attack up to 50°. The emitted fluid technique, as well as tufts and flow cones, were used to document the surface flow. A smoke generator system injected smoke into the vortex cores generated by the forebody and leading-edge extensions (LEXs). Documentation was provided by onboard still photographs and video, by air-to-air photography, and by postflight photography.

The surface flow visualization techniques revealed laminar separation bubbles near the forebody apex, lines of separation on the forebody and LEX, and regions of attached and separated flow on the wings and fins. The off-surface flow visualization techniques showed the path of the vortex cores on the forebody and LEX as well as the LEX vortex core breakdown location. An interaction between the forebody and LEX vortices was noted. The flow over the surfaces of the vertical tail was categorized into regions of attached, unsteady, or separated flow using flow tufts.

17. Key Words (Suggested by Author(s)) Boundary layer transition, F-18, Flow separation, Flow visualization, High angle of attack, Vortices	18. Distribution Statement Unclassified-Unlimited
	Subject category 02

19. Security Classif. (of this report) Unclassified	20. Security Classif. (of this page) Unclassified	21. No. of Pages 41	22. Price A-03